NUREG/CR-5233

A Computer Code for Fire Protection and Risk Analysis of Nuclear Plants

Prepared by A.K. Singhal, S.D. Habchi, A.J. Przekwas

CFD Research Corporation

Prepared for
U.S. Nuclear Regulatory
Commission

NUREG/CR-5233
RP

A Computer Code for Fire Protection and Risk Analysis of Nuclear Plants

Manuscript Completed: June 1988
Date Published: September 1988

Prepared by
A.K. Singhal, S.D. Habchi, A.J. Przekwas

CFD Research Corporation
3313 Bob Wallace Avenue, Suite 205
Huntsville, AL 35805

Prepared for
Division of Engineering
Office of Nuclear Regulatory Research
U.S. Nuclear Regulatory Commission
Washington, DC 20555
NRC FIN D2041

ABSTRACT

A fire modeling computer code has been developed with sufficient flexibility for accurate representations of geometry, ventilation and other conditions as may be present in cable rooms, control rooms, and other enclosures in nuclear power plants. The computer code is capable of three-dimensional, transient, turbulent flow and heat transfer calculations with chemical reaction and radiation. The code has a modular struc-ture, specifically designed for fire problems.

The code employs the latest relevant finite-volume solution techniques. The code has been applied to a series of benchmark problems and a recent fire test problem. This has confirmed the feasibility of the fire code. Considerable further work is needed to enhance the physical models (to improve the realism of predicted solutions) and to validate and document the final code. Specific recommendations are made for Phases II and III of the Project.

TABLE OF CONTENTS

TABLE OF CONTENTS (CONT.)

LIST OF ILLUSTRATIONS

LIST OF ILLUSTRATIONS (CONT.)

LIST OF ILLUSTRATIONS (CONT.)

LIST OF TABLES

1. INTRODUCTION AND SUMMARY

1.1 Background

This is the final report of the SBIR Phase I (six-month) study, entitled: "A Computer Code for Fire Protection and Risk Analysis of Nuclear Power Plants". The study was sponsored by the U.S. Nuclear Regulatory Commission (NRC Contract No. NRC-04-87-374) and conducted by CFD Research Corporation (CFDRC Project No. 4025).

The overall objective of the proposed research program (Phases I, II, and III) is to provide NRC, utilities, and affiliated organizations, with a computer program capable of predicting thermal environments, of postulated fires, inside control rooms, cable rooms, and other enclosures of nuclear power plants. The nature of the analysis is deterministic (rather than probabilistic) and the selected approach is "field modeling" (rather than "zone modeling"). In general, the field modeling approach is known as the Computational Fluid Dynamics (CFD) approach. Typical results of such analyses include three-dimensional, time-dependent distributions of velocity, temperature, pressure, and concentrations of selected species. Such flow details are important for:

1. better understanding of fire environments and their sensitivity to various geometric and ventilation parameters of complex enclosures;
2. improved basis of regulatory requirements (such as those in Appendix R to 10CFR50 and Section 9.5.1 of the Standard Review Plan [1]); and
3. improved design and operation of complex enclosures and their ventilation and fire protection systems.

In the past, several field modeling studies [2-8] have been performed, either with general-purpose proprietary CFD codes or with research codes at Universities. The purpose of the proposed project is to develop and validate a CFD code, **specifically designed for fire modeling problems**, by using the latest relevant numerical techniques and physical models. The code will represent the current state-of-the-art of field modeling of fires, and will be a **practical analysis tool**.

1.2 Objective of Phase I Study

The general objective of SBIR Phase I studies is to establish the feasibility of the proposed approach. For the present study, specific objectives (as stated in the Phase I proposal) are:

1. Design a code architecture to maximize modularity, portability, and ease-of-use.
2. Construct the basic code by meticulous coding of selected techniques and physical models.

3. Perform check-out and verification calculations.
4. Prepare the final report.

1.3 Results of Phase I Study

The Phase I study has met all of the above-stated objectives. A three-dimensional, transient fire analysis computer program has been developed and demonstrated up to the planned stage. It consists of three modules as shown in Figure 1.1.

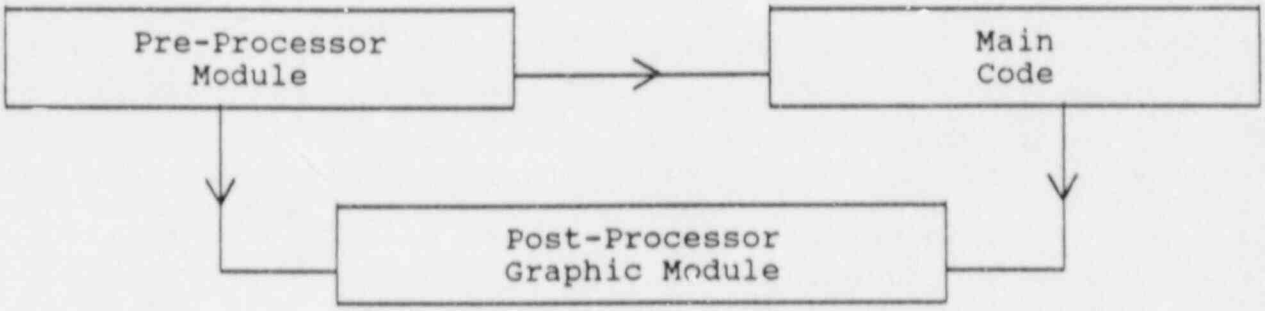

Figure 1.1 Main Modules of the Fire Code

The pre-processor module provides the means to set up a problem in either "interactive" or "batch" mode. It has provisions for geometric prescriptions of complex enclosures, multiple internal solid objects, partitions, and multiple inlets and outlets of the ventilation system. The main code consists of about 20 major subroutines and several subprograms, so as to maximize the modularity of the code. In Phase I work, maximum emphasis has been placed on the selection and implemertation of numerical schemes, as these form the foundation of the code. The selected numerical schemes include:

- A pressure-based, finite-volume solution method.
- A fully implicit formulation, for efficient simulation of transient flows.
- First and second order accurate differencing schemes (the latter is implemented, but not yet tested).
- Iterative, sequential solutions of dependent variables [Each variable is solved for over the whole calculation domain (rather than over a plane, line, or point) before the solution of the next variable starts].
- Use of CFDRC's latest whole-field equation solver with extended, symmetric links (the use of an efficient and robust linear equation solver is important for the overall computational efficiency of solutions).
- Use of modified SIMPLEC algorithm.
- Use of dynamic storage and vectorizable coding practices.

In addition to the above numerical schemes, the code has provisions for the following physical models.

- k-ε turbulence model with modifications for buoyancy effects.
- Multi-scale turbulence models.
- Instantaneous (diffusion-controlled) reaction model
- One-step (global kinetics) reaction model, with modifications for turbulence interaction, such as eddy break-up model.
- Multiple-step (two or four step) reaction model, with provisions for production and reaction of intermediate species such as CO, C_2H_4, etc. As compared to one-step models, a multiple-step model will be more realistic for fires in small enclosures or in low ventilation conditions.
- Six-flux radiation model; this does not require gases to be transparent to radiation, and therefore provides a good basis for radiation in fire/smoke environment.
- Transient heat conduction model, based on an integral profile method to calculate heat losses through thick walls, with proper account of time-dependent temperature profiles and thermal inertia of walls.

The basic k-ε turbulence model and the one-step reaction model have been completed and used in the present demonstration calculations. Most of the other physical models have been incorporated into the code, but not yet debugged or tested. Likewise, the post-processor module of the code is in its initial stage of development, which sufficed to produce basic graphics capability of plotting velocity vectors and contours of temperature, etc., as presented in Sections 4 and 5 of this report.

To verify the developed code, several bench-mark problems have been simulated. These problems include:

1. Driven Cavity Problem
2. 2-D Plane Flow Over a Backward Step
3. Developing Turbulent Pipe Flow
4. 2-D Axisymmetric Flow Over a Backward Step
5. 2-D Natural Convection in a Square Enclosure
6. 3-D Natural Convection in a Closed Enclosure
7. Shear Mixing Layer (Propane-Air Non-Reacting)

Each of the above problems includes at least one critical physical phenomenon of typical fire problems. Results of these simulations have been found to be satisfactory (i.e. in agreement with benchmark data).

For the demonstration of the code's capability of simulating nuclear power plant fire problems, the code was also applied to a recent (1986/87) fire test problem (selected from the fire tests conducted at the Factory Mutual Research Corporation, under the guidance of Sandia National Laboratory on behalf of the U.S. Nuclear Regulatory Commission). Reference 9 provides sample data for three tests using propylene gas as fuel. The test enclosure

is 60'×40'×20' and has a ventilation system with one exhaust and six inlet ports. Test #4 has been used as the base case in the present study. The ventilation rate for this case is one room change per hour. At present, for demonstration purposes, walls have been assumed to be adiabatic, and a coarse grid has been used. The three-dimensional calculations have been made for 0-6 minute durations. Fire has been simulated by prescribing mass source of fuel (rather than directly prescribing heat release rate) and using a one-step chemical reaction model. The initial results show qualitatively plausible flow distribution. However, the predicted temperature profile, along a vertical line near the fire source, did not show very good agreement with the measured data. To determine contributing factors for this discrepancy, several two-dimensional investigatory calculations have been performed. It is established that finer computational mesh and improved boundary conditions (e.g. convective and radiative heat transfer to walls) are needed to improve the agreement of predictions with experimental data, to a satisfactory level. Improvements in other physical models are also important, however, for the selected test case, these will contribute to a relatively smaller extent. Several additional two-dimensional calculations have also been made to examine the sensitivity of solutions to: (a) internal solid obstacle; (b) wider exhaust outlet; (c) alternative practice of simulating ventilation air inlet; and (d) increased ventilation flow rate. Results of these parametric calculations showed physically correct trends, and confirmed the basic soundness of the developed fire code.

1.4 Recommendations for Phase II Work

The work completed in Phase I has clearly established the feasibility of an advanced state-of-the-art fire simulation code. To convert this code into a **reliable and usable code** (i.e. fully validated and well-documented code), the following work items are recommended for SBIR Phase II study.

1. Completion and testing of the physical models (described in Section 1.3).
2. Systematic parametric studies to establish the sensitivity of results to computational mesh, and various physical models.
3. Validation of the code against several (at least six) test cases of the 1986-87 NRC/SNL/FMRC experiments. If necessary, additional data from earlier tests (published by SNL, NBS, EPRI, FRS (UK), etc.) will also be used.
4. Finalization of the code, with emphasis on the ease-of-use, modularity, and portability.
5. Documentation of the code (including all assumptions, theoretical models, code structure and user's guide).

A detailed work plan with time and cost estimates will be submitted to NRC in the SBIR Phase II proposal.

1.5 Recommendations for Phase III Work

After the satisfactory completion of Phase II work, to effectively utilize and disseminate the developed code, the following three activities are recommended to be carried out with commercial and/or non-SBIR government funds.

1. Incorporation of selected data bank, i.e. physical properties and models for typical fire sources, pertinent to nuclear power plants.
2. Enhancement of graphical display of results (improved color graphics and animation of results) so that the time evolution of the fire environments can be presented (and recorded) in the form of movies and/or video cassettes. Such films (real-time results) will enhance the general use of results, and will also be very useful in assessing various safety aspects such as available evacuation time.
3. Development of technical training and user support material, and a provision for code maintenance and necessary enhancements.

For items 1 and 2 above, necessary support will be sought from commercial organizations such as: Factory Mutual, Ove Arup & Partners, and IBM. In the past, these organizations have shown positive inclinations, however, due to the uncertainty and delay in NRC's request for 1988 SBIR proposals, no formal agreements have been established.

For item 3 above, CFDRC plans to provide the necessary support from its internal funds.

1.6 Outline of the Remainder of the Report

Following this Introduction and Summary section, Section 2 discusses the mathematical background of the numerical and physical models and solutions procedure. Section 3 describes salient features of code structure and overall logic. Section 4 describes verification test cases and results. Section 5 describes the results of a fire demonstration problem (selected from 1986/87 fire tests of FMRC/SNL/NRC) and several investigatory test cases to support the analysis of results. Conclusions drawn from the present study and recommendations for future work are presented in Section 6.

2. MATHEMATICAL BACKGROUND

2.1 Introduction

The fire code predicts fluid flow, heat transfer, and chemical reaction processes in a three-dimensional cartesian or cylindrical domain by solving a system of governing transient, partial differential transport equations. Objectives and capabilities of

the code have been described in Section 1. This chapter describes the mathematical formulation of the selected equations and the assumptions in physical models and relevant numerical techniques.

2.2 Governing Equations

The general form of the conservation equations is as follows:

$$\frac{\partial \rho\phi}{\partial t} + \text{div}\ (\rho\vec{v}\phi) = \text{div}\ (\Gamma_{eff}\ \text{grad}\ \phi) + S_\phi \qquad (1)$$

Where ϕ stands for general conserved property like the velocity components (u, v, w), the enthalpy (h), the turbulence kinetic energy (k) and its dissipation rate (ϵ), the mass fraction of the fuel (m_{fu}), and various species concentration C_i. All variables represent time-averaged, rather than instantaneous, values of a turbulent flow. The variables ρ, $\vec{v}$, and S_ϕ stand for density, velocity vector, and source term for ϕ per unit volume respectively. Finally, Γ_{eff} is the effective exchange coefficient for the transport of property ϕ. The values for different Γ_{eff} and S for different ϕ's are listed in Table 1.

In the present study, variable-density forumulation is used, i.e. the Boussinesq approximation in not used. Local density is used in all convection and source terms. The buoyancy term $g(\rho - \rho_{ref})$ in the v-momentum equation implies that the reduced (or relative) pressure practice is used. For buoyancy-dominated flows, this practice is known to be superior to the practice of using absolute pressure (or ρg as the buoyancy term). The local density, ρ, is calculated from the equation of state as a function of local temperature and local species composition.

The following three equations apply to Table 1 and define the effective and turbulent viscosities and the turbulence generation rates G_k and G_b:

$$\mu_{eff} = \mu_t + \mu_l \qquad (2)$$

$$\mu_t = C_\mu \rho k^2/\epsilon \qquad \text{and} \qquad (3)$$

$$\begin{aligned} G_k = \mu_t \Bigg\{ & 2\left[\left(\frac{\partial u}{\partial x}\right)^2 + \left(\frac{\partial v}{\partial y}\right)^2 + \left(\frac{\partial w}{\partial z}\right)^2\right] \\ & + \left[\left(\frac{\partial u}{\partial z}\right)^2 + \left(\frac{\partial w}{\partial x}\right)^2\right] + \left[\left(\frac{\partial w}{\partial y}\right)^2 + \left(\frac{\partial v}{\partial z}\right)^2\right] \\ & + \left[\left(\frac{\partial u}{\partial y}\right)^2 + \left(\frac{\partial v}{\partial x}\right)^2\right] \Bigg\} \end{aligned} \qquad (4)$$

Table 1. Exchange Coefficient (Γ) and Source Term (S_ϕ) for Different ϕ Variables

Dependent Variable	Exchange Coefficients	Source Terms
ϕ	Γ_ϕ	S_ϕ
1	0	0 (Continuity)
u	μ_{eff}	$-\frac{\partial p}{\partial x} + \frac{\partial}{\partial x}\left(\mu_{eff}\frac{\partial u}{\partial x}\right) + \frac{\partial}{\partial y}\left(\mu_{eff}\frac{\partial v}{\partial x}\right) + \frac{\partial}{\partial z}\left(\mu_{eff}\frac{\partial w}{\partial x}\right)$
v	μ_{eff}	$-\frac{\partial p}{\partial y} - g\left(\rho - \rho_{ref}\right) + \frac{\partial}{\partial x}\left(\mu_{eff}\frac{\partial u}{\partial y}\right) + \frac{\partial}{\partial y}\left(\mu_{eff}\frac{\partial v}{\partial y}\right) + \frac{\partial}{\partial z}\left(\mu_{eff}\frac{\partial w}{\partial y}\right)$
w	μ_{eff}	$-\frac{\partial p}{\partial z} + \frac{\partial}{\partial x}\left(\mu_{eff}\frac{\partial u}{\partial z}\right) + \frac{\partial}{\partial y}\left(\mu_{eff}\frac{\partial v}{\partial z}\right) + \frac{\partial}{\partial z}\left(\mu_{eff}\frac{\partial w}{\partial z}\right)$
h	$\frac{\mu_{eff}}{\sigma_h}$	$\dot{q}'''$
k	$\frac{\mu_{eff}}{\sigma_k}$	$G_k + G_b - \rho\epsilon$
ϵ	$\frac{\mu_{eff}}{\sigma_\epsilon}$	$\frac{\epsilon}{k}\left[\left(G_k + G_b\right) - \rho\epsilon\right]$
C_i	$\frac{\mu_{eff}}{\sigma_i}$	R_i

$$G_b = \frac{\mu_t}{\rho} g \frac{\partial \rho}{\partial z} \quad (5)$$

The term G_b, in the sources of k and ϵ equations, represents the buoyancy effect on turbulence [6]. This term is incorporated into the code, but was not activated in the present development/ demonstration computations, reported in Sections 4 and 5 of this report.

2.3 Description of Physical Models

The physical models of turbulence, heat transfer, combustion, and radiation selected and incorporated into the fire code have been outlined in Section 1. The Salient features of these models are described below.

Turbulence Model: Two turbulence models are incorporated in the fire code:

- The k-ϵ model of turbulence [10], with modifications for buoyancy terms [5].
- The multiple scale turbulence model of Chen and Kim [11].

The basis of the k-ϵ model has been well documented [10] and the model has been verified on a variety of nonreactive and reactive flow problems. It involves solution of two transport equations for: kinetic energy of turbulence, k, and turbulence dissipation rate, ϵ. The source terms for these equations, as shown in Table 1, involve semi-empirical constants which are assigned the following standard values.

$$C_1 = 1.44,$$
$$C_2 = 1.92,$$
$$C_\mu = 0.09,$$
$$\sigma_k = 1.0, \text{ and}$$
$$\sigma_\epsilon = 1.3$$

The major shortcoming of the k-ϵ model is its inability to predict the response rate to changes in main field strain rates. Computational study for flows in homogeneous turbulence in the uniform shear flow showed that the k-ϵ model correctly predicted the asymptotic level of turbulence, but the predicted time to reach that level was an order of magnitude longer than the experimental one.

Recently, several works on the multiple scale turbulence (MST) model have been conducted. One of the most advanced ones has been recently presented by Chen and Kim [11]. The MST model subdivides the kinetic energy of turbulence into two regions: The large scale (or production) region, k_p, and the small (dissipa

tive) scale region, k_t. The partitioning, as shown in Figure 2.1, is determined as a part of the solution and depends on local turbulence intensity, production, transfer, and dissipation rate. The partition is moved into higher wave numbers when production is high, and to low wave numbers when production vanishes. The source terms for the set of four equations are:

$$S_{k_p} = G - \rho \epsilon_p$$

$$S_{k_t} = \rho (\epsilon_p - \epsilon_t)$$

$$S_{\epsilon_p} = \left(C_{p1} \frac{G^2}{\rho \epsilon_p} + C_{p2} G - C_{p3} \rho \epsilon_p \right) \frac{\epsilon_p}{k_p} \qquad (6)$$

$$S_{\epsilon_t} = \rho \left(C_{t1} \epsilon_p \frac{\epsilon_p}{\epsilon_t} + C_{t2} \epsilon_p - C_{t3} \epsilon_t \right) \frac{\epsilon_t}{k_t}$$

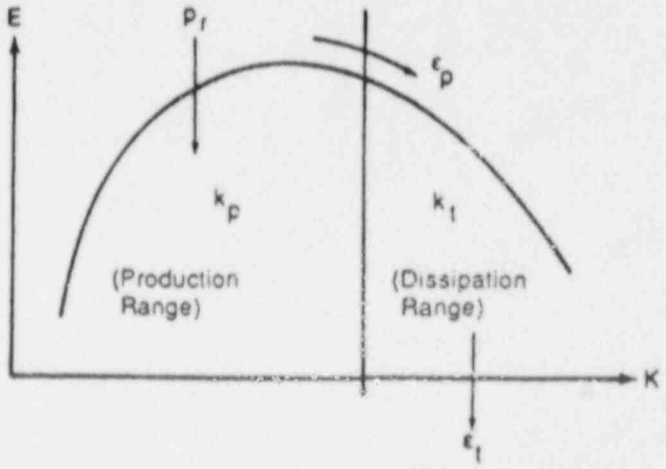

Figure 2.1. Partitioning of the Turbulence Energy Spectral Density in the Multiple Scale Turbulence Model

The total kinetic energy of turbulence is calculated as the sum of both scales, viz:

$$k = k_p + k_t \qquad (7)$$

and the constitutive equation for turbulent viscosity is:

$$\mu_t = C_\mu \rho \, k^2 / \epsilon_p \qquad (8)$$

The turbulence constants for the MST model are:

$\sigma_{kp} = \sigma_{kt} = .75$; $\sigma_{\epsilon p} = \sigma_{\epsilon t} = .75$; $C_\mu = 0.09$; $C_{p1} = 0.21$;
$C_{p2} = 1.24$; $C_{p3} = 1.84$; $C_{t1} = 0.29$; $C_{t2} = 1.28$; $C_{t3} = 1.66$.

The MST model has been tested so far only for nonreactive flows. It is currently being verified for reactive flows in conjuction

with the eddy breakup model. It is planned to use the model in the second stage of the project.

Heat Transfer Model: The basic energy equation is the conservation of stagnation enthalpy $\tilde{h}$ which is defined as:

$$\tilde{h} = h + \tfrac{1}{2} (u^2 + v^2 + w^2) \qquad (9)$$

The second term on RHS is the kinetic energy and it is generally important only for high-velocity (compressible) flows, for the fire code this term is neglected. The static enthalpy, h, is defined as:

$$h = \Sigma\ m_j\ h_j \qquad (10)$$

where m_j is the j-th species mass fraction, and summation is taken over all species within the mixture composition. The static enthalpy of individual species is prescribed as input or can be computed within the code based on the JANNAF tables, as:

$$h_j = h^{\circ}_{f,298K} + \int_{298}^{T} CpdT \qquad (11)$$

An iterative process is required to compute the temperature, T, from known enthalpy, h, because of the nonlinear relationship between them.

At present, thermal boundary conditions can be either of prescribed heat flux or prescribed wall temperature. An important addition, to be made in the Phase II of the project, is to incorporate a transient heat conduction model for accurate calculation of wall heat losses through solid walls. This model will be based on integral profile method and has already been successfully demonstrated in an earlier NRC/BNL study performed by the principal investigator of this project.

Combustion Model: The principal equation used in the combustion model is the conservation equation for chemical species which has the form:

$$\frac{\partial}{\partial t} (\rho m_j) + \mathrm{div}(\rho \vec{u} m_j) = \mathrm{div}(\Gamma_{eff,j}\ \mathrm{grad}\ m_j) + R_j \qquad (12)$$

where m_j is the mass fraction of chemical species j, R_j is the mass rate of reaction of species j due to combustion per unit volume, and $\Gamma_{eff,j}$ is the effective exchange coefficient for species j.

At present, there are two different options considered for the reaction rate R_j:

- One-step Arrhenius reaction model; and
- Eddy-break-up model.

The Arrhenius reaction rate for fuel can be written as:

$$R_{fu} = -\rho A M_{FU} \left(\frac{\rho\ m_{FU}}{M_{FU}}\right)^{\alpha} \left(\frac{\rho\ m_{OX}}{M_{OX}}\right)^{\beta} \exp\left(-\frac{E}{RT}\right) \tag{13}$$

where A is the reaction rate constant, E is the activation energy, R is the gas constant, M_{FU} and M_{OX} are molecular weights of fuel and oxygen, and α and β are reaction order constants. This model is mainly used for kinetically controlled chemical reactions.

For most of the turbulent flows in which mixing is the controlling parameter, the eddy-break-up model of Spalding [12] modified by Magnussen [13] is usually used. The reaction rate for fuel is written as:

$$R_{fu} = -C_R\ \rho g^{\frac{1}{2}}\ \epsilon/K \tag{14}$$

where C_R is an empirical constant and g represents the local mean-square concentration fluctuations, which is expressed algebraically as follows [13]:

$$g^{\frac{1}{2}} = \min\left(m_{fu},\ \frac{M_{OX}}{s},\ \frac{B m_{pr}}{1+s}\right) \tag{15}$$

where B=4.5 is a constant.

Provisions for more complex reaction models such as two or four-step reaction models with intermediate species such as CO, C_2H_4, etc. are also needed in the fire code, particularly for under-ventilated and/or small room fires.

Successful modeling of combustion systems depends on a correct description of the chemical reactions involved. While the complete chemical kinetics of C_nH_m oxidation are not fully understood, there are models available which are more sophisticated than those currently used in the present demontration study. One of these is a four-step kinetic mechanism for hydrocarbon combustion. The results of Hautman [14] indicated the viability of representing the C_nH_{2n+2} - aliphatic hydrocarbon oxidation in a simplified kinetics scheme in the form:

$$C_n\ H_{2n+2} \rightarrow \frac{n}{2}\ C_2\ H_4 + H_2 \tag{16}$$

$$C_2\ H_4 + O_2 \rightarrow 2CO + 2H_2 \tag{17}$$

$$CO + \tfrac{1}{2}\ O_2 \rightarrow CO_2 \tag{18}$$

$$H_2 + \tfrac{1}{2}\ O_2 \rightarrow H_2O \tag{19}$$

where C_2H_4 represents a class of olefinic intermediates. The above reactions are controlled by reaction rate constants which are expressed as:

$$R_{fu} = -10^x [fu]^a [O_2]^b [C_2H_4]^c \exp(-E/RT) \quad (20)$$

$$R_{C_2H_4} = -10^x [C_2H_4]^a [O_2]^b [fu]^c \exp(-E/RT) \quad (21)$$

$$R_{CO} = -10^x [CO]^a [O_2]^b [H_2O]^c \exp(-d\phi) \exp(-E/RT) \quad (22)$$

$$R_{H_2} = -10^x [H_2]^a [O_2]^b [C_6H_4]^c \exp(-E/RT) \quad (23)$$

where x, a, b, c, and d are constants which are different for each reaction, ϕ is the equivalence ratio, E is the activation energy, and R is the universal gas constant.

In the second phase of the project, various advanced reaction models will be reviewed again and suitable one(s) will be utilized.

Thermal Radiation Model: The radiation transport equation for an absorbing-emitting gray medium in local thermodynamic equilibrium can be written as [15]:

$$\vec{\Omega} \cdot \Delta I_r = -aI_r + a\frac{E}{\pi} + \frac{s}{4\pi}\int_{4\pi} I d\Omega \quad (24)$$

where $\vec{\Omega}$ is the unit vector representing direction of radiating beam, I is the radiation intensity, a is beam absorption, s is scattering coefficient, $E=\sigma T^4$ where σ is the Bolzman Constant. A flux model is used to solve the above integro-differential equation where the flux model is the assumed radiation of intensity with direction. Assumption of constant I in a quandrant centered along each (±) coordinate direction results in six differential equations for intensities. Therefore, this model is known as the six-flux radiation model. This model has been used, successfully in several reactive flow simulations [16, 17].

2.4 Description of Numerical Procedure

A finite-volume approach based on the modified SIMPLEC algorithm [18, 19, 20] has been used in the fire code. The code has provisions for cartesian (x, y, z) and cylindrical (x, y, θ) coordinates. Grid distributions can be non-uniform to accommodate finer grid spacings in the regions of steep flow gradients. Internal solid blockages due to, say, cabinets, cables, partitions, etc. are represented by using the "partial porosity" (or "porosity-resistivity") approach.

The fire code uses a staggered grid practice in the so-called "backward boomerang" mode, shown schematically in Figure 2.2. The velocity components are calculated at the cell faces while all other scalar variables are calculated at the grid center.

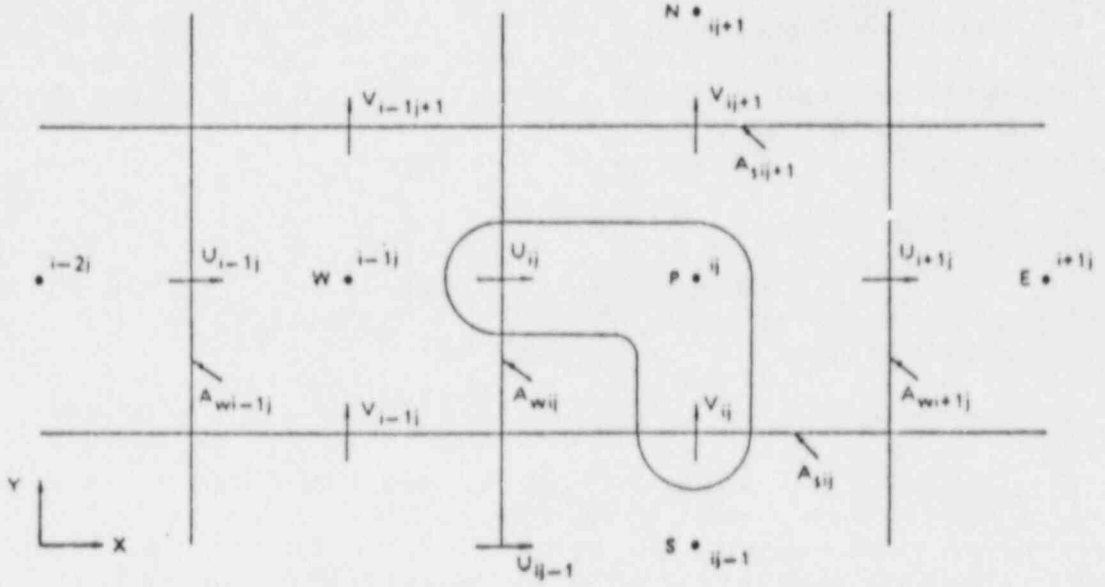

Figure 2.2 Staggered Grid Notation in the x-y Plane

There are six types of geometrical boundary conditions that can be specified in the fire code.

- Fixed mass flow rate inlets that can account for forced or free multiple ventilation inlets;
- Fixed pressure inlets or exits;
- Solid wall boundaries;
- Symmetry planes;
- Internal mass sources without momentum; and
- Zero gradient boundaries such as adiabatic walls.

Special attention is required for the near wall boundary conditions. For velocities, classical wall functions, based on the logarithmic low of wall, are used. Near wall turbulence parameters, that are based on the assumption of local equilibrium between total turbulence kinetic energy and second scale dissipation rate, are assumed. For the energy equation, prescribed wall temperature or heat flux boundary conditions are used. As mentioned earlier, in Phase II, a transient heat conduction model for solid walls will be incorporated. This will enable coupled solution of heat transfer between gas and solid regions.

Finite-Volume Differencing Scheme: The partial differential equations (1) are integrated over the finite volume, and for transient calculations, over the finite time interval to obtain the descretized equations. A hybrid formulation is used for convection and diffusion terms. This formulation has proven to be very robust, but does lead to significant numerical diffusion

of solutions. Therefore, a more advanced (second-order accurate) scheme, i.e. central differencing with second and fourth-order dissipation terms, is also included in the code. The second-order scheme will be tested in Phase II work.

For transient calculations, a fully implicit formulation is employed where the values of flow variables are taken to be those which prevail at the current time step (backward Euler formulation). Integration of the partial differential equaitons results in linear algebraic equations of the form:

$$a_p\phi_p = a_E\phi_E + a_W\phi_W + a_S\phi_S + SU_\phi + M^\circ\phi_p^\circ \qquad (25)$$

where a_E, a_W, ..., etc. are called "link coefficients", SU and SP are the linearized sources, M° is the accumulation term, and a_p (diagonal coefficient) is expressed as:

$$a_p = a_E + a_W + a_N + a_S - SP_\phi + M^\circ \qquad (26)$$

Solution Procedure: A set of linearized equations, one equation for each variable at each grid node, needs to be solved for each time step. These equations are coupled with each other because of the presence of several dependent variables in each equation. Also, since the original partial differential equations are non-linear, the linearized equations need to be solved iteratively with under-relaxation. The required under-relaxation and number of iterations strongly depend upon the manner in which the equations are solved. In the present code, the following practices have been chosen.

1. Equations are solved in a successive (variable-by-variable) manner.
2. Each variable is solved for over the whole calculation domain (rather than over a plane or a line) before the solution of the next variable starts.
3. Provisions are made for the solutions by:
   a) an iterative whole-field (3-D) solver, and
   b) Jacobi Point-by-Point solver.

The selected whole-field solver [21] is a modified version of Stone's Implicit Procedure [22], and is considerably more efficient especially for ill-conditioned and non-symmetric matrices. At least, the pressure-correction equations are solved by using this equation solver. This equation plays a central part (and consumes major computational effort) in the selected solution scheme. The solution of other variables, such as velocities, can be equally efficient (depending upon the various versions of the SIMPLE algorithm) by the whole-field or point-by-point solution.

An inertial under-relaxation practice is employed for all dependent variables except pressure. This practice is achieved

by adding an inertia term, viz: $I_\phi(\phi-\phi^*)$ to the finite difference equation in the following manner:

$$\phi = \frac{\Sigma a_n \phi_n + SU + I_\phi \phi^*}{\Sigma a_n - SP + I_\phi} \tag{27}$$

where suffix ,n, denotes all cell neighbors, and superscript ,*, denotes the previous iteration value of ϕ. The "inertia term" ,I_ϕ, is calculated as:

$$I_\phi = \frac{\rho \ VOL}{\Delta t_{F\phi}} \tag{28}$$

where ρ is the fluid density, VOL is the grid cell volume and $\Delta t_{F\phi}$ is the "false" time step specified for each dependent variable ϕ. Typically Δt_F is specified to be of the order of resident time of fluid in a typical control volume. It should be noted that in converged solutions $\phi \to \phi^*$, and therefore the addition of the inertia term does not affect the final solution.

In order to monitor the convergence of the iterative solution procedure, the residual errors are calculated for the equations of all dependent variables and at each control cell, in the following manner:

$$\epsilon_{\phi p} = \Sigma a_n \phi_n + SU - SP\phi_p^* - (\Sigma a_n)\ \phi_p^* \tag{29}$$

where $\epsilon_{\phi p}$ stands for the residual error in the equation of variable ϕ at point p, and summation is taken over all link coefficients: N, E, W, S, ..., etc.

The residual errors are used as indicators for the convergence of the solution. Generally, the sum of absolute values of residuals for each variable are required to reduce approximately by three orders of magnitude. In Phase II, after the experience of several fire test problems, specific recommendations and built-in convergence criterion will be provided.

3. CODE STRUCTURE

During the process of designing the structure of the fire code, maximum emphasis was placed on the modularity and the ease of use. For these purposes, the computer code was divided into three interconnected modules as previously shown in Figure 1.1.

The pre-processor module provides the means to set up the test case in either interactive or "batch" mode. It allows specification of the geometry, grid, and boundary conditions, solution and printout control, etc. Provisions are also made in the preprocessor for providing physical properties data. The pre-processor overall structure is shown in Figure 3.1.

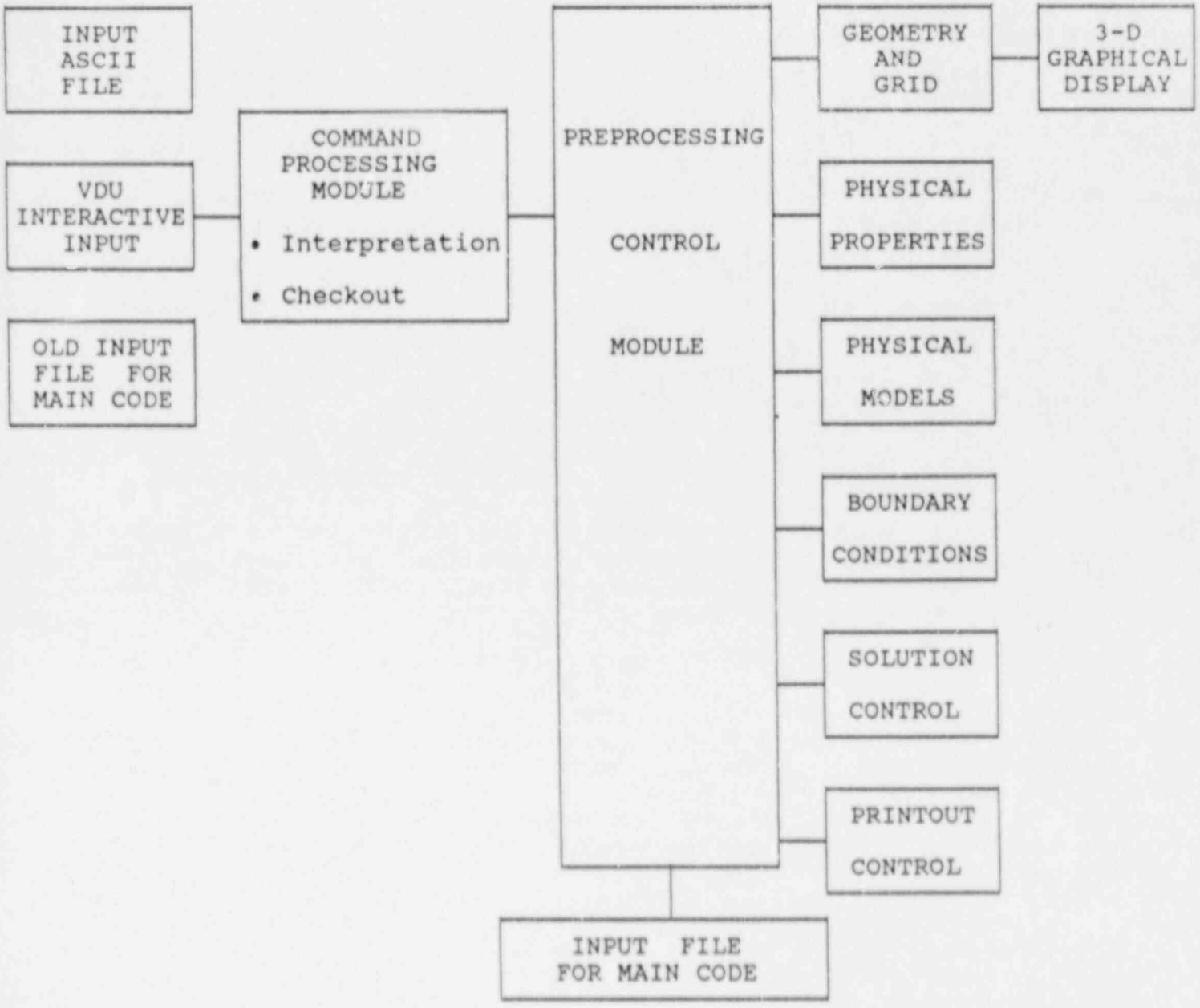

Figure 3.1 Structure of the Pre-Processor

The main code module (Equation Solver) includes a large number of subroutines, each with specific functions such as treatment of boundary conditions, grid and geometry, initial field, physical properties, physical models, solution algorithm and output control. Major parts of physical models are coded in self-contained, modular subroutines. This module also includes a subroutine for dumping the data to files for further (restart) analysis and/or graphical post processing of selected flow fields.

The post-processor module is prepared as a separate program that has access to the data files generated by the main code and the pre-processor modules. Graphical display of grid and geometry, velocity vectors, contours of all variables, and profiles are available through an interactive mode in the post-processor.

An overall structure of the main code and the post-processor is shown in Figure 3.2. Further details, such as functions and detailed flow charts of all major subroutines will be provided in the final report of Phase II work.

4. CODE VERIFICATION STUDY

4.1 Overview

The selected solution scheme and physical models have been used successfully in many codes, including several written by the members of the present project team. However, before a code can be used for engineering analysis, it must be checked out/verified systematically for a large number of problems of increasing complexity. This section summarizes the verification problems which have so far been simulated with the fire code.

1. Two-dimensional driven cavity flow with different Reynolds numbers.
2. Laminar flow over a backward-facing step.
3. Developing turbulent pipe flow.
4. Two-dimensional axisymmetric turbulent flow over a backwark-facing step.
5. Two-dimensional natural convection in an enclosed cavity, with different Rayleigh numbers ($10^3 \leq Ra \leq 10^7$).
6. Three-dimensional natural convection in an enclosed cavity (room with hot and cold walls).
7. Shear mixing layer (propane-air non-reacting).

All cases were selected because each of them contains at least one flow feature which is likely to be present in fire problems. For cases 1, 2, 3, 4, 5, and 7 bench-mark data are available for quantitative comparisons. Case 6 was performed mainly to check the code capability for three-dimensional buoyancy-dominated flow. This case is designed to have symmetric boundary conditions such that the calculated flow field can be examined for the symmetry conditions.

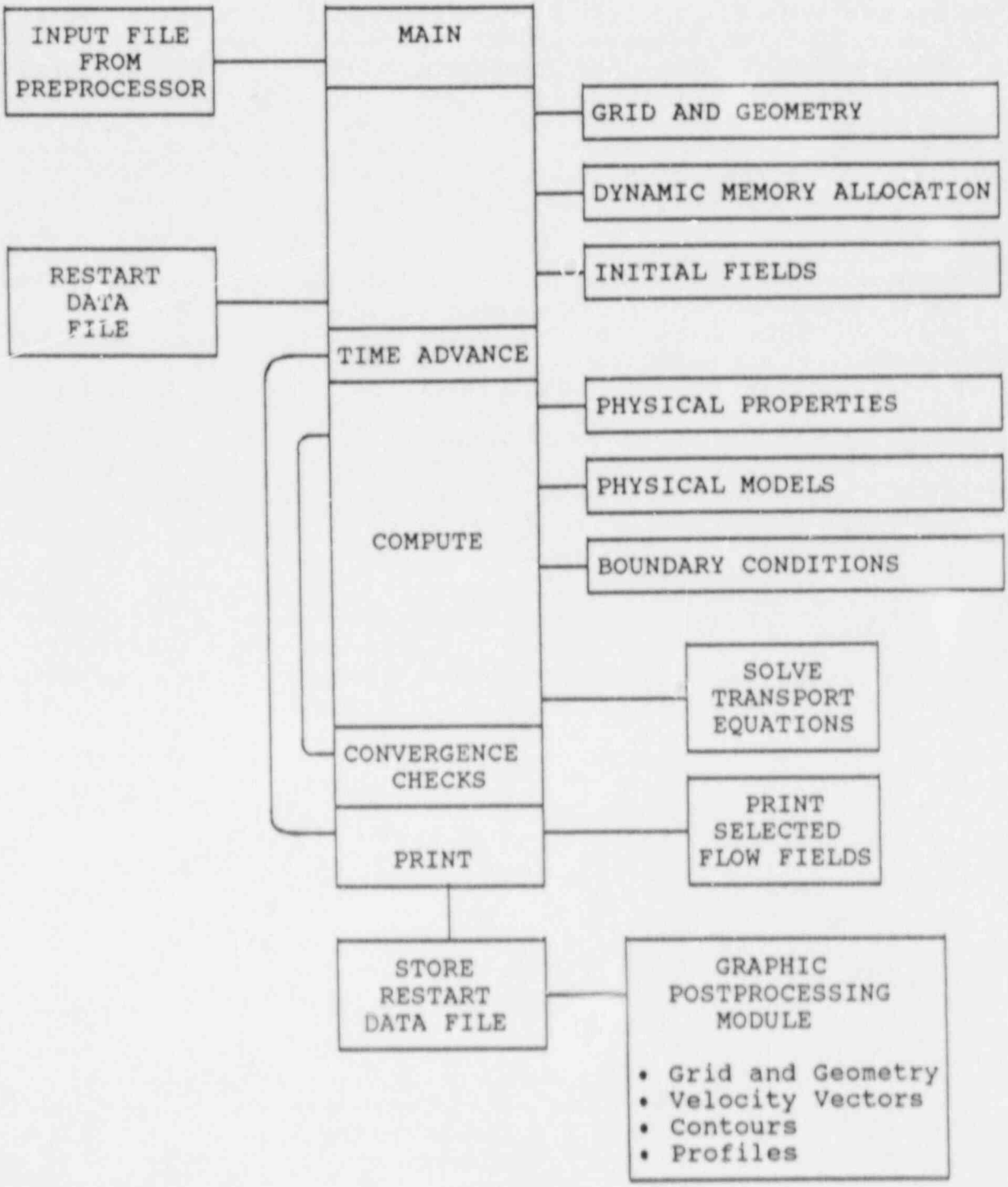

Figure 3.2 Structure of the Main Code

In the following sections, the verification problems are briefly described and their results are presented.

4.2 Two-Dimensional Driven Cavity Flow

The driven cavity problem is a good test case for two-dimensional elliptic flows. In this problem, the top wall of the cavity moves at a constant velocity while the remaining three walls are stationary (no-slip boundaries). The geometry is illustrated in Figure 4.1. A sample computational grid with uniformly distributed 80 grid cells in the x-direction and 80 grid cells in the y-direction is shown in Figure 4.1.

Computations have been performed with several grids in the range of 10 × 10 to 120 × 120, with uniform and non-uniform distributions, for three Reynolds numbers (i.e. Re=100, 1000, and 10000).

Results for Re=1000 case are presented in Figure 4.2. The streamline contours show the expected recirculation pattern with a big central vortex and two secondary weak vortices in the corners. These results have been compared to the bench-mark solutions reported by Ghia, et. al. [23], who solved the same problem with 257 × 257 grid points. The comparison between Figures 4.2a and 4.2b indicate a good agreement. Further improvement in accuracy is expected with the use of a second-order differencing scheme (in Phase II). Similar agreements were obtained at the two other Reynolds numbers.

4.3 Two-Dimensional Laminar Flow Over a Backward-Facing Step

In this case, analysis of laminar flow over a backward-facing step with 1:2 expansion ratio was performed. The geometry and computational grids are shown in Figure 4.3. The computational grid used consisted of 120 grid cells in the x-direction and 40 grid cells in the y-direction. The grid was clustered near the step and in the expected recirculation zone. The inlet location was chosen such that, based on a uniform inlet velocity profile, the flow is fully developed when it reaches the step.

Results were obtained for Re=100 and Re=378. For Re=100, the predicted reattachment length was found to be x/h=2.7 which is within five percent of the experimental data reported by Armaly, et. al. [24]. For Re=398, the fire code overpredicted the reattachment length by about eight percent. The axial velocity profiles for both cases (Re=100, 398) are shown in Figure 4.4 and they indicate good agreement with the data reported in Reference 23.

4.4 Developing Turbulent Pipe Flow

In this verification case, the developing turbulent flow in a pipe is simulated. The geometry of the pipe is depicted in Figure 4.5. The length of the pipe, L, was chosen such that the

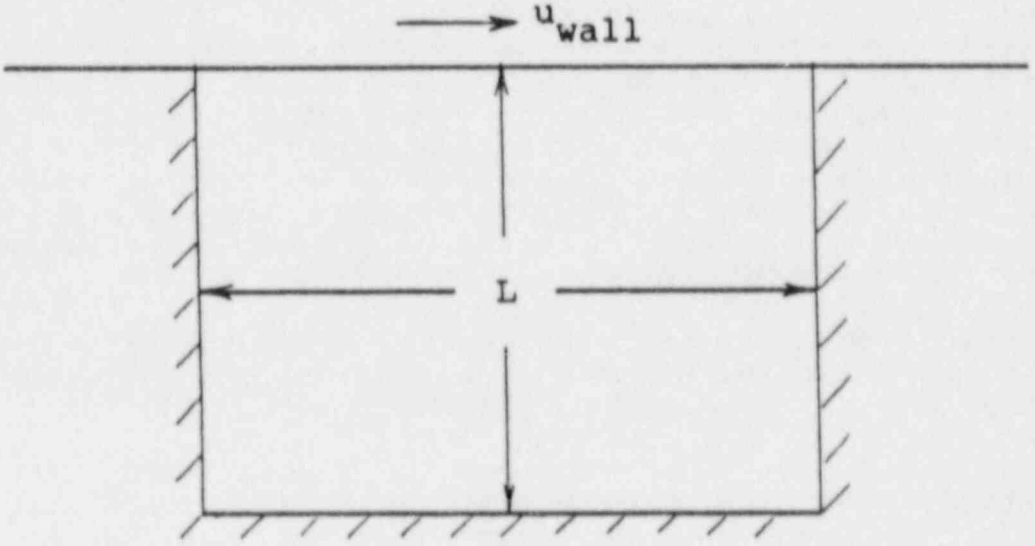

(a)

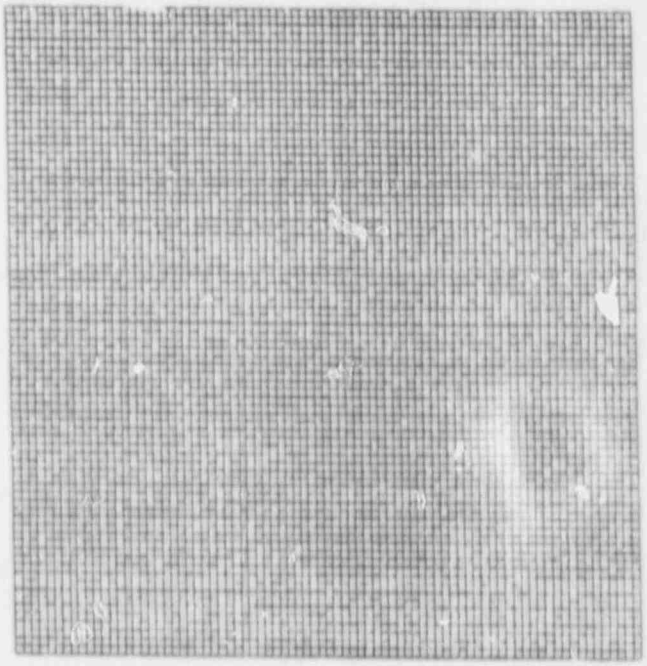

(b)

Figure 4.1 Geometry and Computational Grid for Driven Cavity Problem

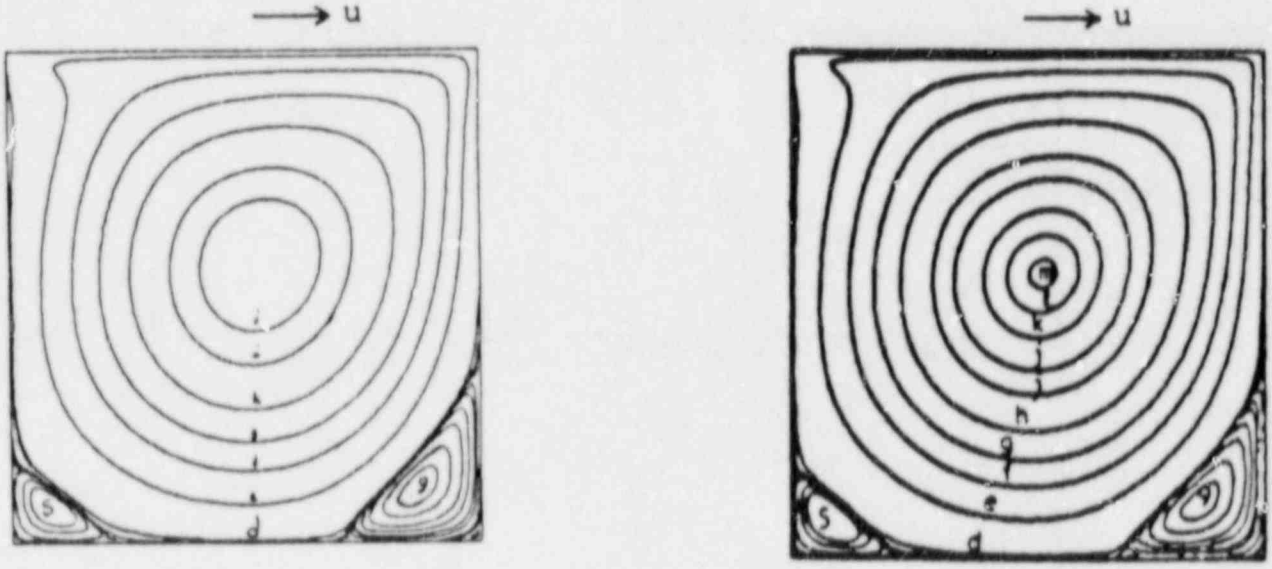

(a) (b)

Stream function			
Contour letter	Value of ψ	Contour number	Value of ψ
a	-1.0×10^{-10}	0	1.0×10^{-8}
b	-1.0×10^{-7}	1	1.0×10^{-7}
c	-1.0×10^{-5}	2	1.0×10^{-6}
d	-1.0×10^{-4}	3	1.0×10^{-5}
e	−0.0100	4	5.0×10^{-5}
f	−0.0300	5	1.0×10^{-4}
g	−0.0500	6	2.5×10^{-4}
h	−0.0700	7	5.0×10^{-4}
i	−0.0900	8	1.0×10^{-3}
j	−0.1000	9	1.5×10^{-3}
k	−0.1100	10	3.0×10^{-3}
l	−0.1150		
m	−0.1175		

Figure 4.2 Streamline Contours from, a) Present Fire Code; b) Ghia, et. al. [23]

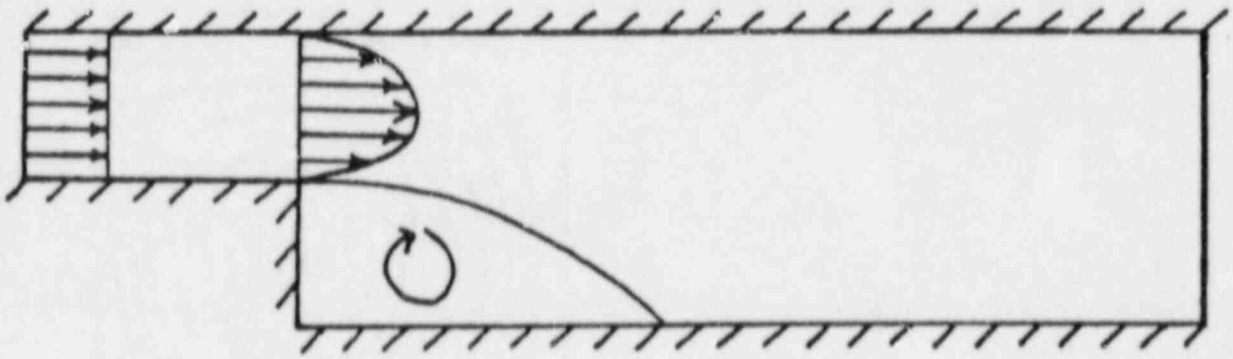

(a)

* Note that both graphs are not to scale

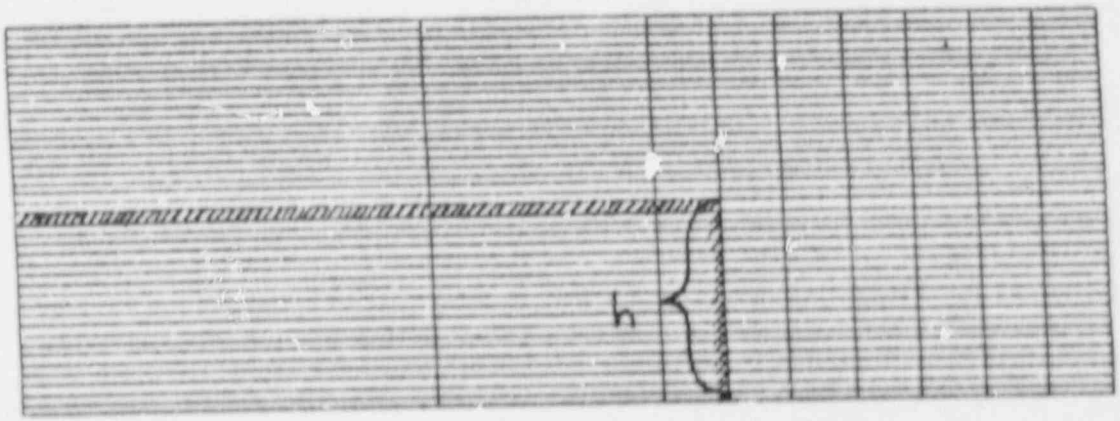

(b)

Figure 4.3 Magnified Inlet Region of Backward-Facing Step: a) Geometry, and b) Computational Grid

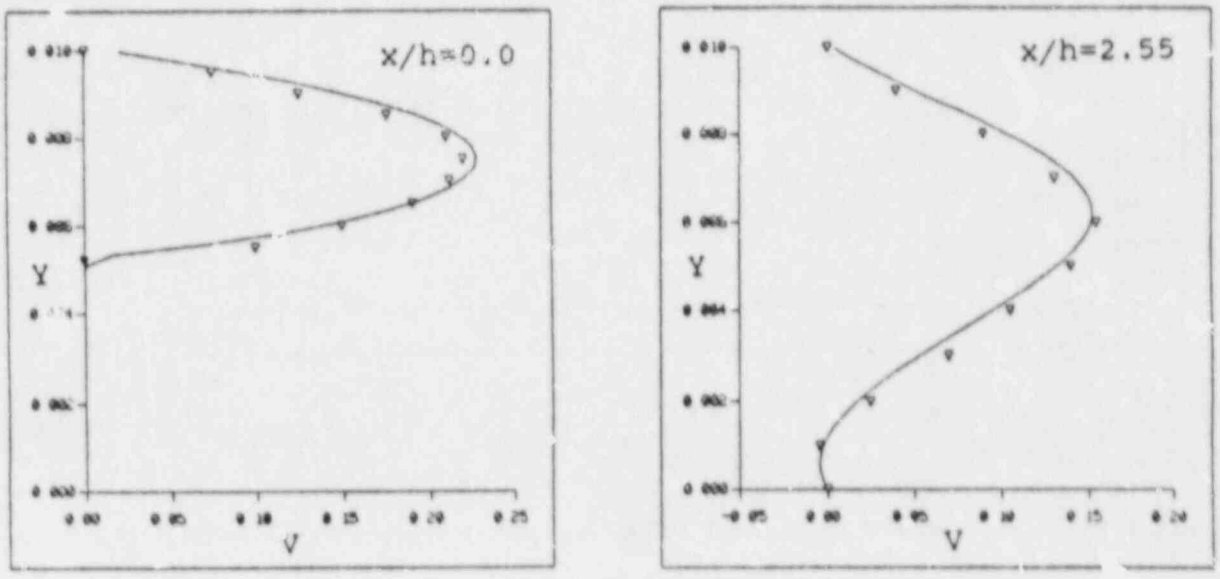

Re = 100

——— Predicted

▽ Experimental [24]

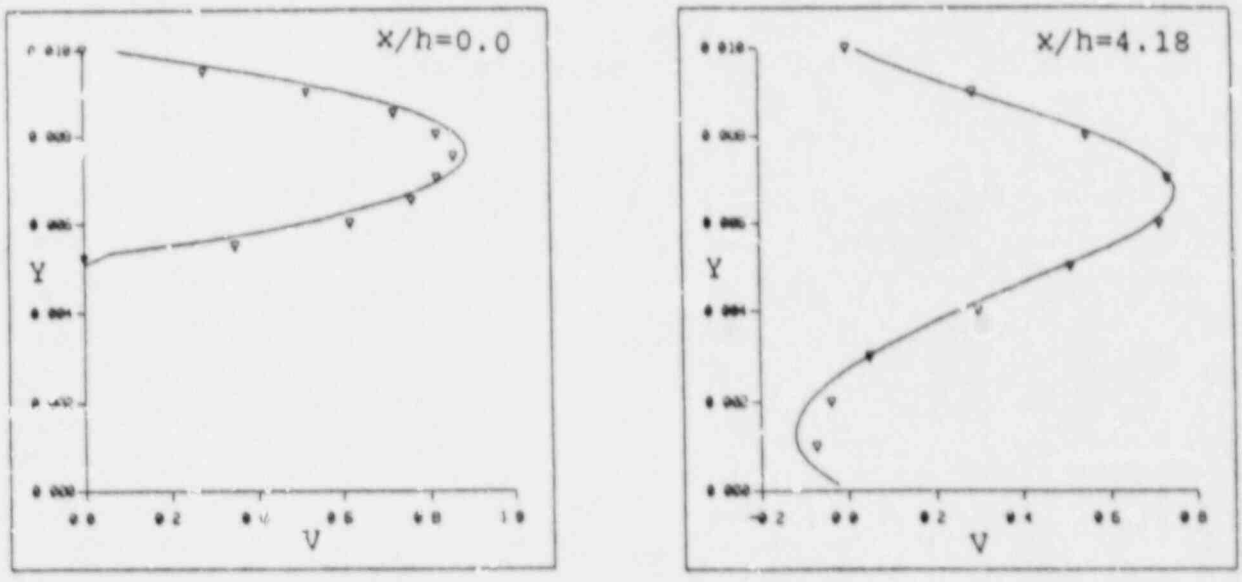

Re = 358

Figure 4.4 Comparison of Predicted Axial Velocity Profiles with Experimental Data of Armaly, et. al. [24]

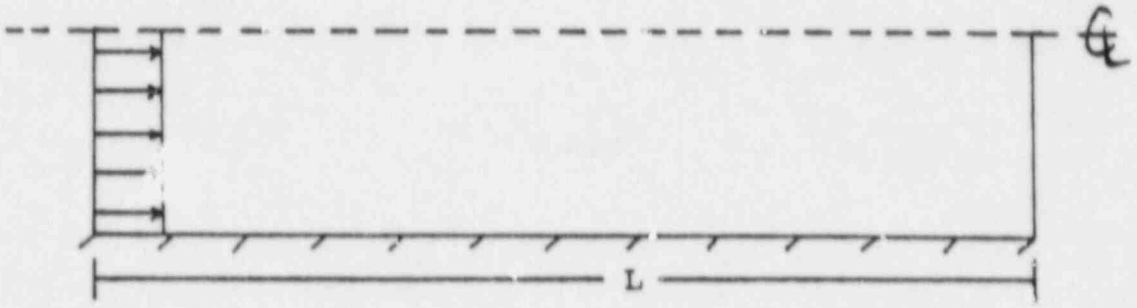

Figure 4.5 Geometry of the Developing Pipe Flow Problem

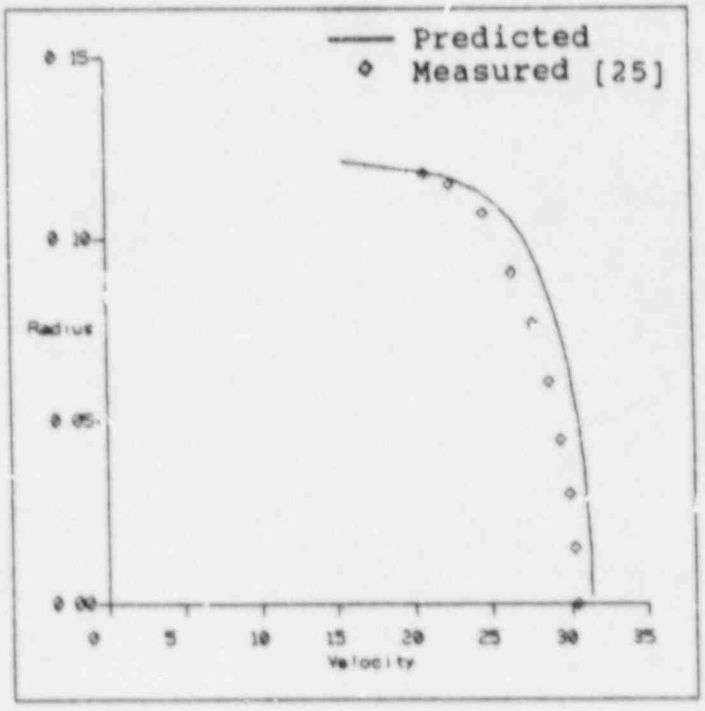

Figure 4.6 Predicted and Measured Axial Velocity Profile for Fully Developed Turbulent Pipe Flow

flow gets fully developed downstream. The standard k-ϵ model was used to obtain results for $Re=5\times10^5$. The velocity profile in the fully-developed region is presented and compared to the experimental results of Laufer [25] in Figure 4.6. The comparison indicates satisfactory agreement.

4.5 Two-Dimensional Axisymmetric Flow Over a Backward-Facing Step

Two-dimensional non-swirling turbulent flow over an axisymmetric backward-facing step is considered in this case, as shown in Figure 4.7. Results were obtained, using the k-ϵ turbulence model for $Re=1.25\times10^5$. The axial velocity profiles in the fully developed region (before the step) and at $x/h=2.0$ are shown in Figure 4.8 and compared to the experimental data of Samimy, et. al. [26]. As shown in both figures, the fire code predictions have good agreement with the experimental data.

4.6 Two-Dimensional Natural Convection

In this verification case, flow in an enclosed square cavity with differentially heated walls is considered. The geometry and boundary conditions of the computational domain are shown in Figure 4.9. The horizontal (top and bottom) walls are insulated ($\partial T/\partial y = 0$) while the vertical walls are held at constant temperatures,

$$T = T_h \quad \text{at} \quad x = 0$$

and

$$T = T_c \quad \text{at} \quad x = L.$$

Results were obtained for Rayleigh numbers of $Ra=10^3$, $Ra=10^5$, and $Ra=10^7$. Velocity vectors for $Ra=10^5$ are shown in Figure 4.10. Streamline and temperature contours for three different Rayleigh numbers are shown in Figures 4.11 and 4.12, respectively. For $Ra=10^3$, the streamlines are smooth and no distinct boundary layer can be determined. As the Rayleigh number increases, secondary recirculation eddies form as shown in Figure 4.10 ($Ra=10^5$, $Ra=10^7$) and a significant temperature gradient develops near the walls (Figures 4.12b and 4.12c).

The predicted behavior of the flow depicted in Figures 4.11 and 4.12 is identical to the benchmark results published in the literature by G. DeWahl Davis [27] and others.

4.7 Three-Dimensional Natural Convection

The geometry and computational grids for this three-dimensional problem are shown in Figure 4.13. The grid size employed consists of 30 grid cells in the horizontal x-direction, 30 grid cells in the vertical y-direction, and 10 in the z-direction. Boundary conditions are comprised of zero wall velocities and

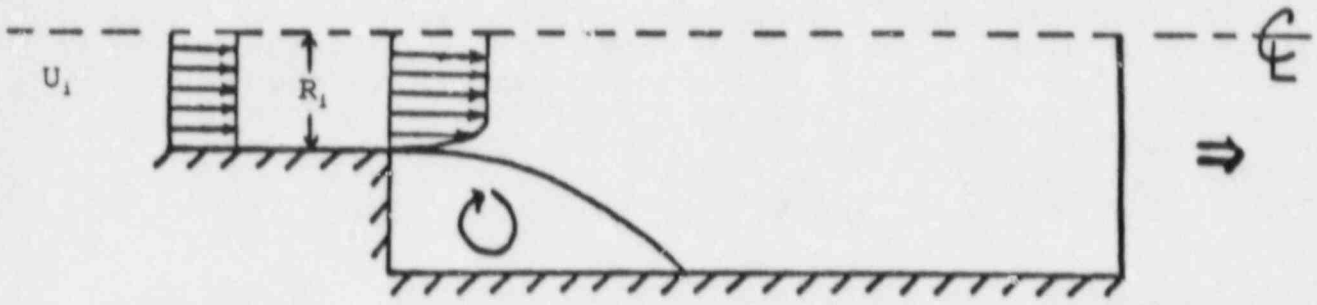

Figure 4.7 Geometry of the Inlet Section of the 2-D Axisymmetric Backward-Facing Step Problem

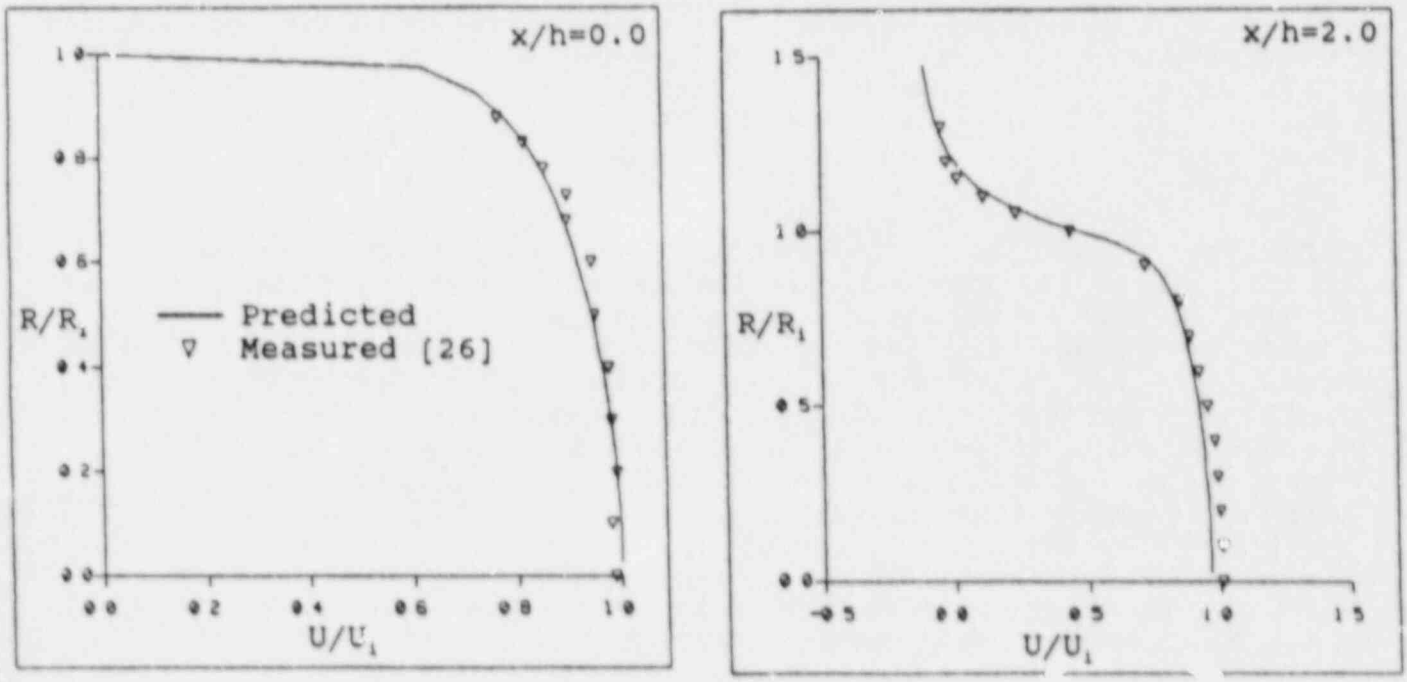

Figure 4.8 Predicted and Measured Axial Velocity Profiles

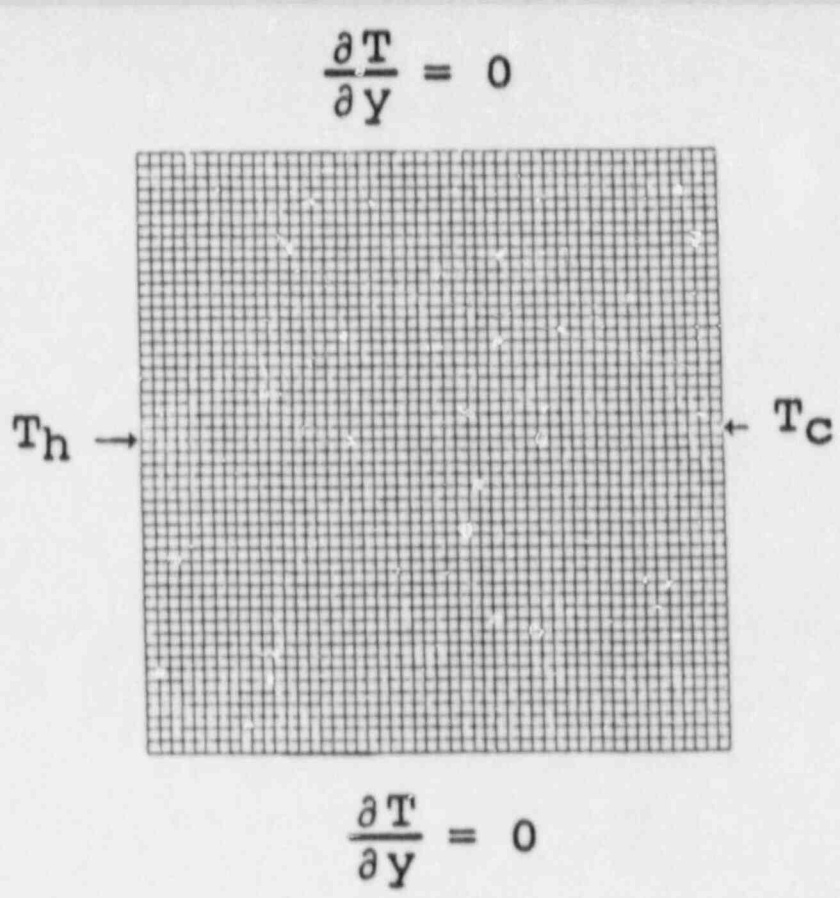

Figure 4.9 Grid and Boundary Conditions for 2-D Natural Convection Problem

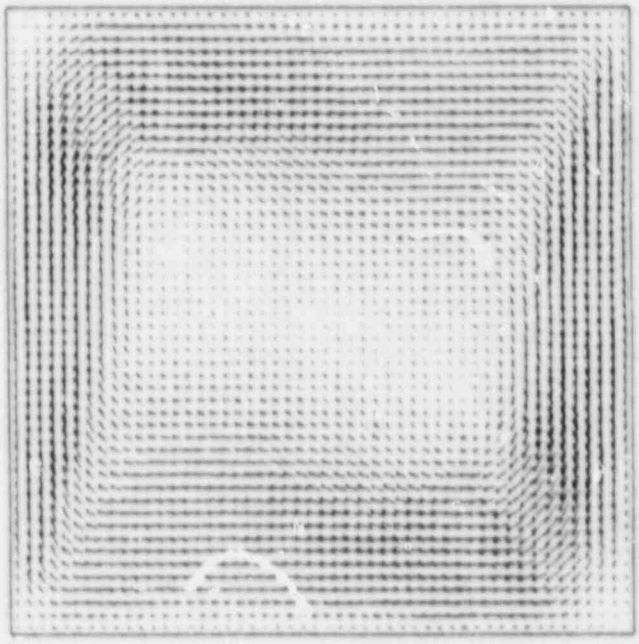

Figure 4.10 2-D Natural Convection Velocity Vectors for $Re=10^5$

(a)

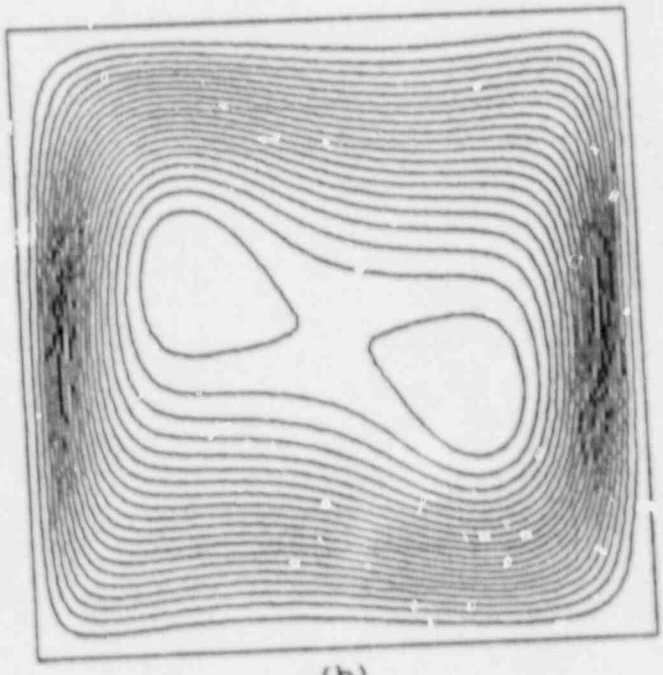

(b)

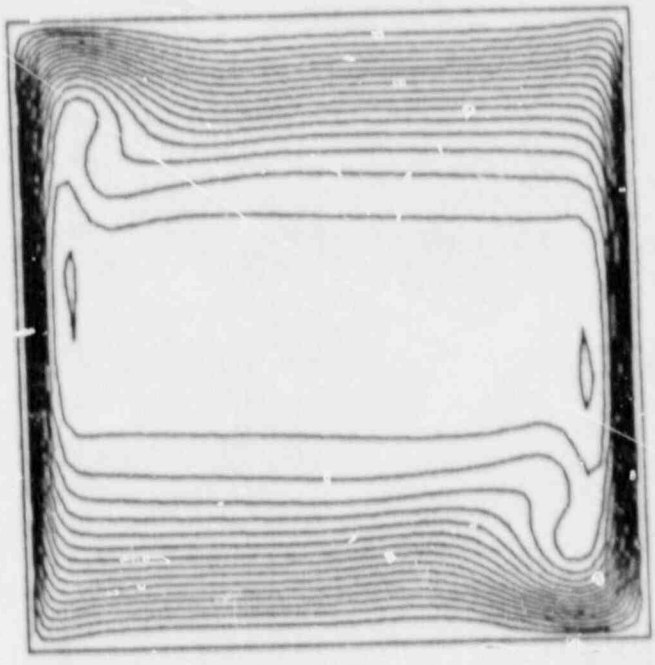

(c)

Figure 4.11 Streamlines in a Square Enclosure for a) $Ra=10^3$; b) $Ra=10^5$; c) $Ra=10^7$

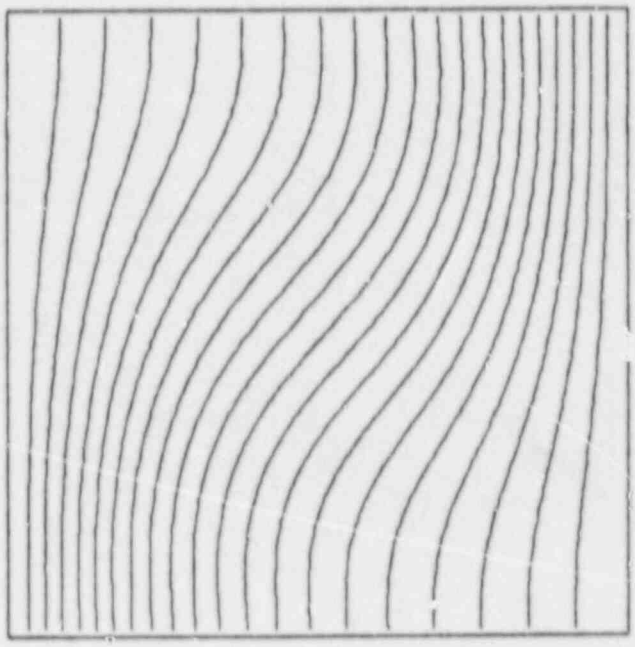

(a)

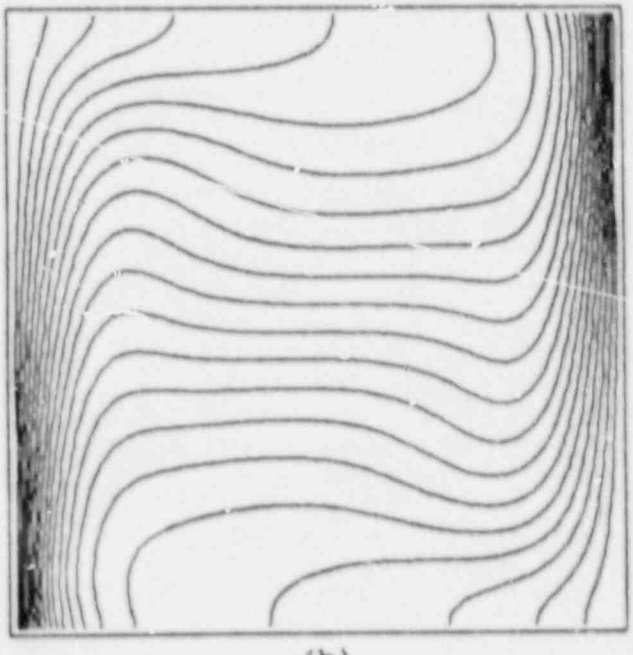

(b)

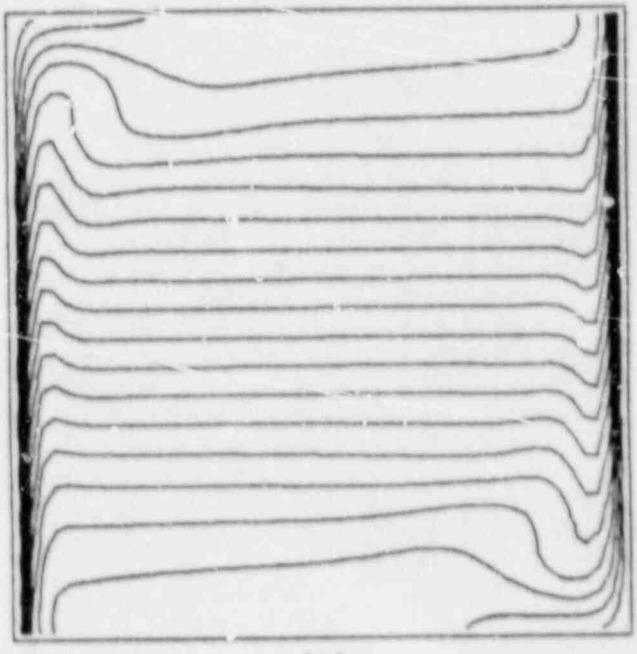

(c)

Figure 4.12 Temperature Contours in a Square Enclosure for a) $Ra=10^3$; b) $Ra=10^5$; c) $Ra=10^7$

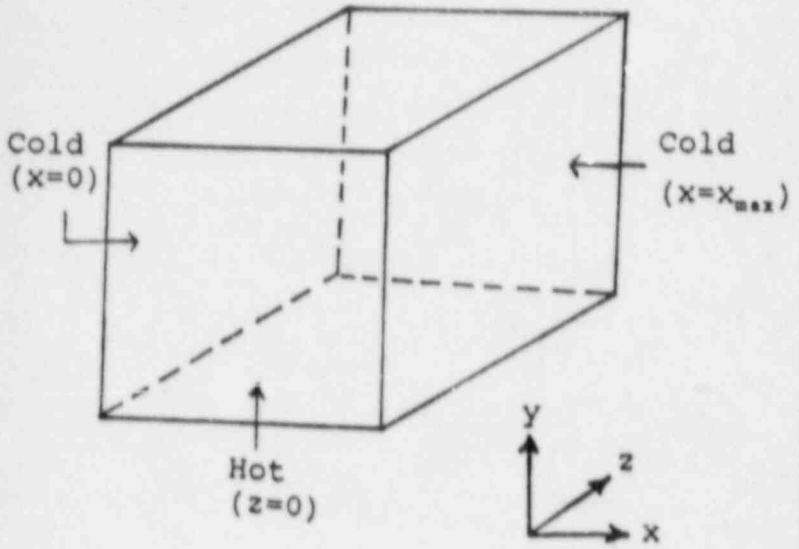

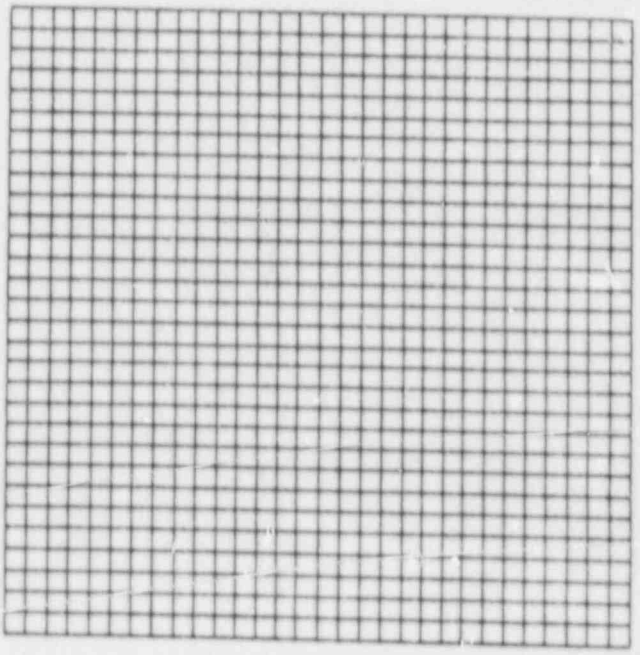

x-y Plane

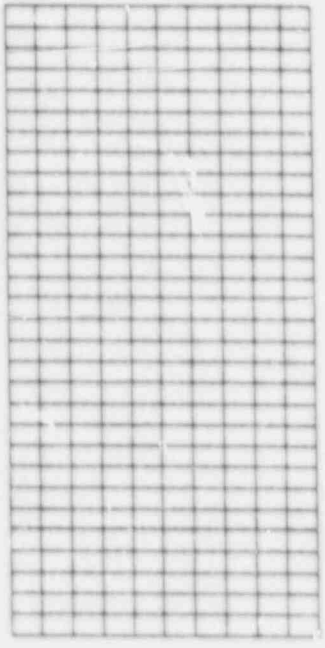

y-z Plane

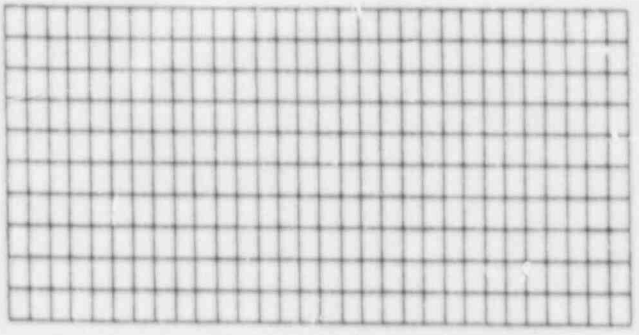

x-z Plane

Figure 4.13 Grid and Geometry for 3-D Natural Convection Problem

prescribed wall temperatures and zero heat fluxes, specified as follows:

Cold Walls: $T(x=0,y,z) = T_c$,

$T(x=L,y,z) = T_c$,

Adiabatic Walls: $\frac{\partial T(x,y=0,z)}{\partial y} = 0$,

$\frac{\partial T(x,y=M,z)}{\partial y} = 0$,

Hot Wall: $T(x,y,z=0) = T_h$, and

Symmetry Plane: $\frac{\partial \phi\ (x,y,z=N)}{\partial z} = 0$.

As in the previous case, the flow here is dominated by the buoyancy force. As the temperature near the hot wall (z=0) increases, the fluid becomes less dense, creating a buoyancy force resulting from density difference. The buoyancy force acts vertically upward and causes the less dense fluid to rise as shown in Figure 4.14a. The opposite happens near the two vertical cold walls because the fluid is more dense, therefore it falls near both walls creating two circulating eddies near the middle of the room as shown in Figure 4.14b. Since the flow rises near the hot vertical plane, it falls near the symmetry vertical plane as shown in Figure 4.14c. Figure 4.15 shows the velocity vectors in two horizontal planes where the flow is directed toward the hot wall near the bottom plane and away from the hot wall near the top wall. Figure 4.16 shows the velocity vectors in three vertical YZ planes. Near the cold wall, the flow is falling as expected while some recirculating motion is observed in the middle of the room.
Temperature contours in three planes are shown in Figure 4.17. The contours in the mid-vertical plane indicate that the hottest fluid is near the middle of the room, away from the cold walls. Figures 4.17b and 4.17c show the highest isotherms near the hot wall as expected.

4.8 Shear Layer Mixing (Propane-Air Non-Reacting)

In this last verification case, the problem of turbulent non-reacting propane-air jets flow was considered. The geometry and the computational grids are shown in Figure 4.18. The computational grid consisted of 20 grid cells in the radial direction, where 5 cells were placed within the inner jet and 15 cells within the outer jet. The horizontal x-direction was modeled by

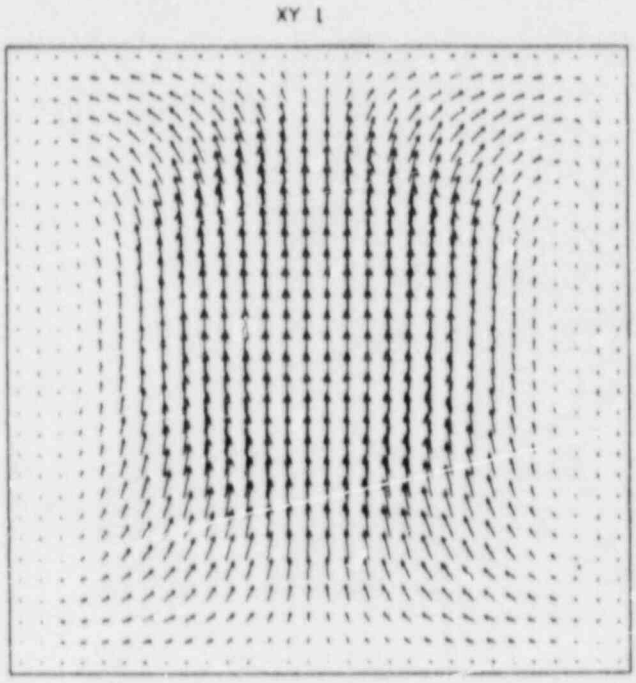

(a) Near Hot Plane

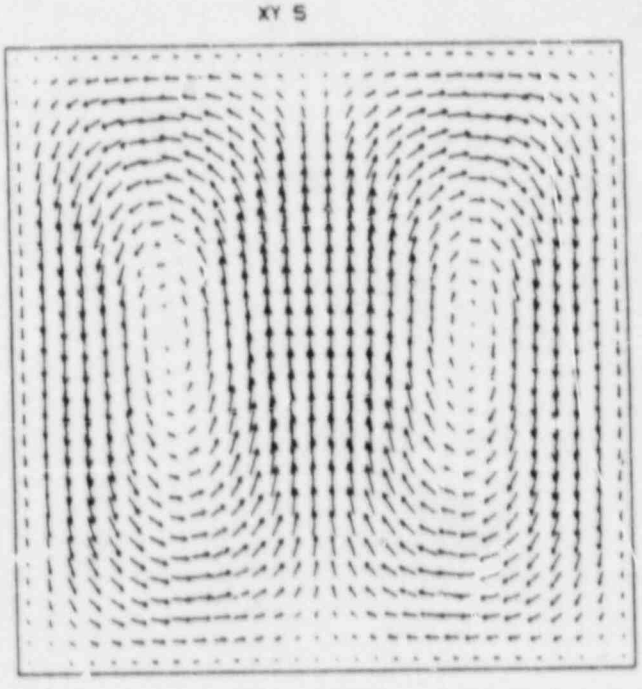

(b) Mid-Vertical Plane

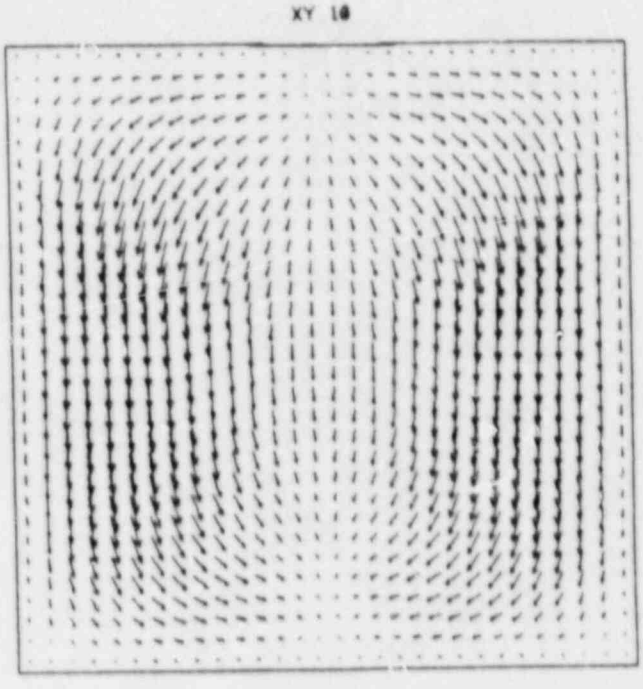

(c) Near Symmetry Plane

Figure 4.14 Predicted Vertical (xy) Velocity Distribution for the 3-D Natural Convection Problem

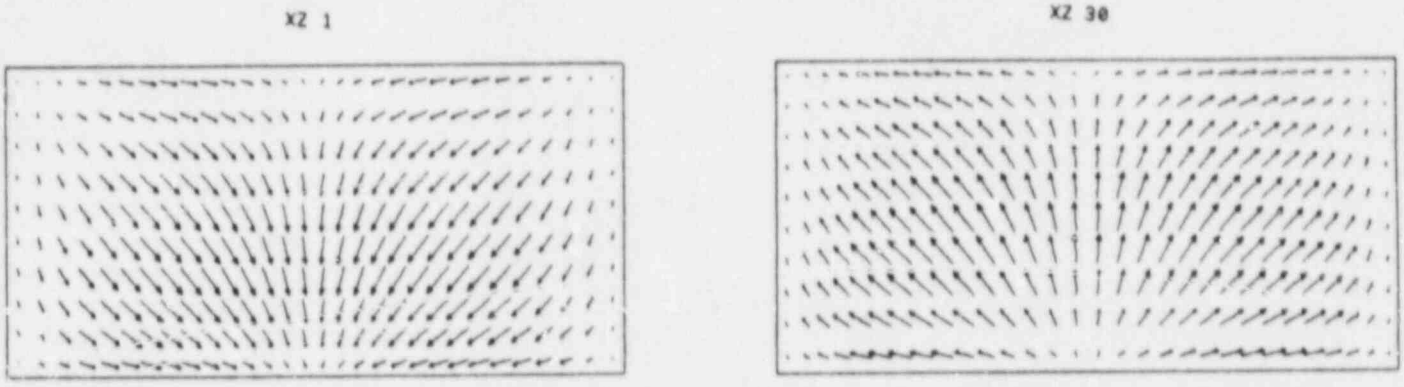

Bottom Plane

Top Plane

Figure 4.15 Predicted Horzontal Velocity Distribution for 3-D Natural Convection Problem

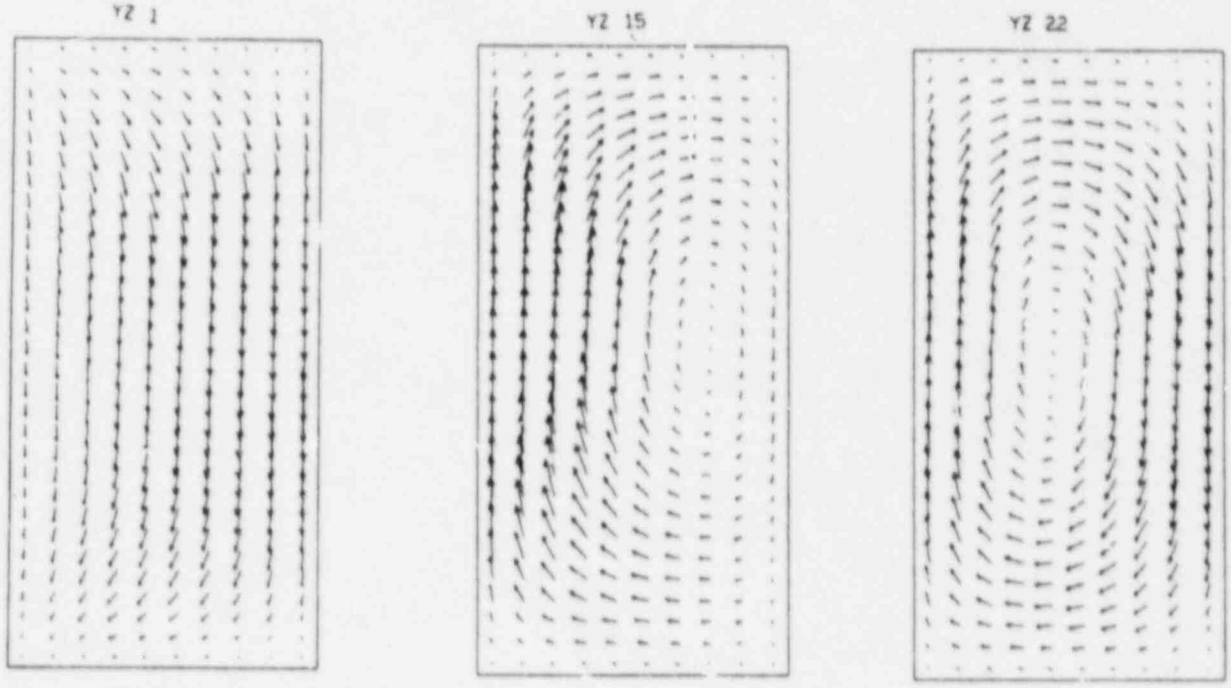

Figure 4.16 Predicted "ertical (yz) Velocity Distribution for 3-D Natural Convection Problem

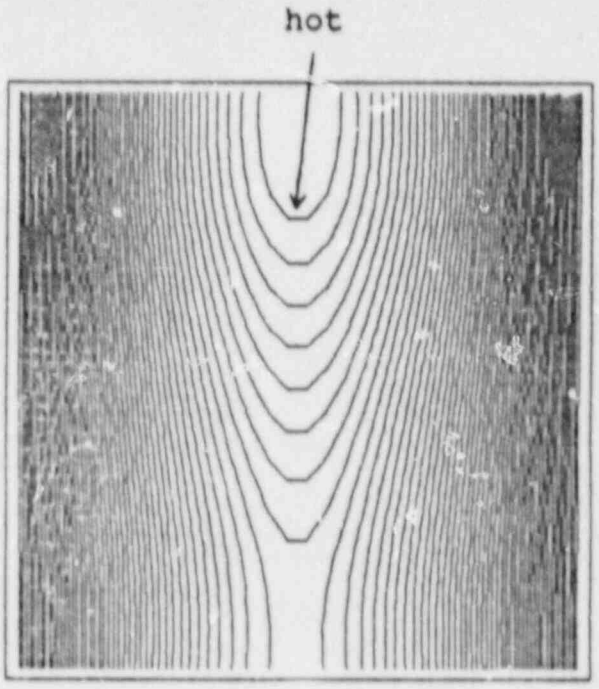

a) vertical (XY) plane, parallel to hot wall

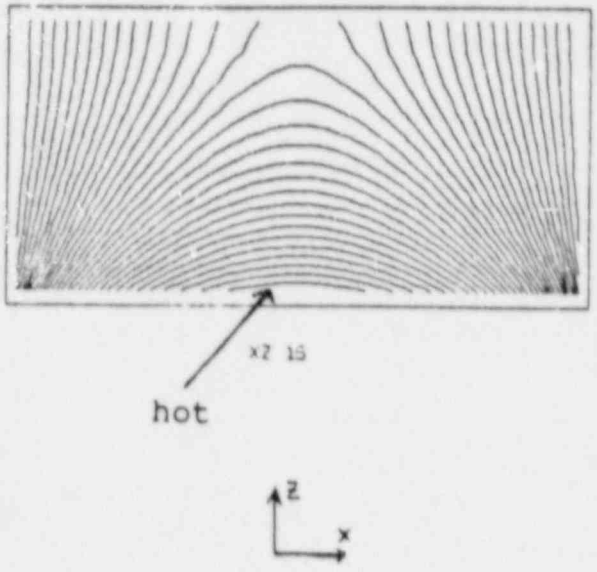

b) horizontal (XZ) plane

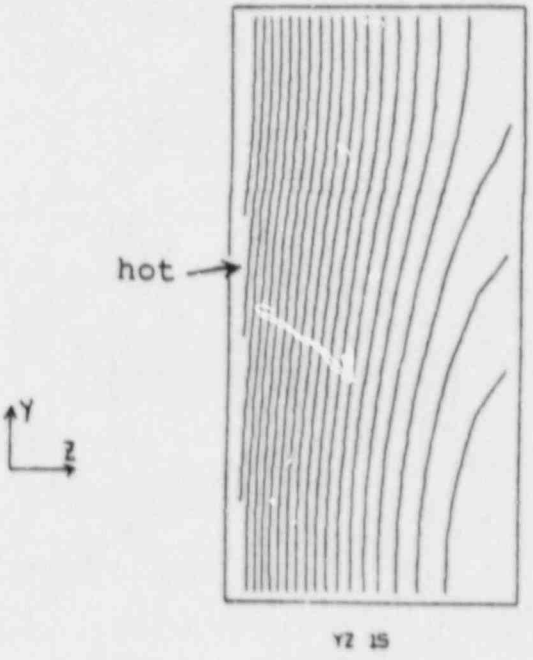

c) vertical (YZ) plane, parallel to cold walls

Figure 4.17 Calculated Isotherms in Three Mid Planes

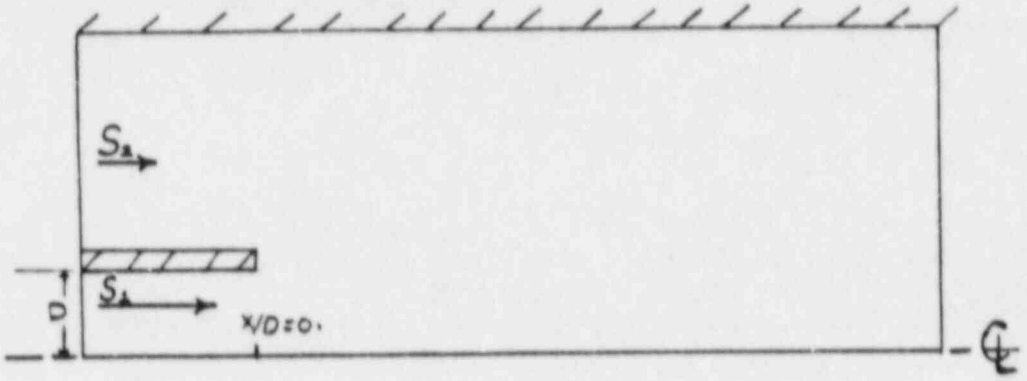

Geometry

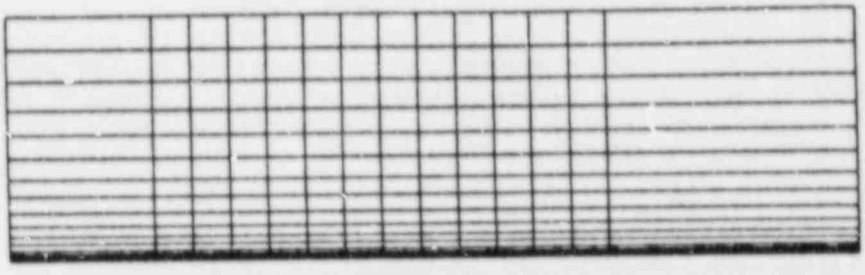

20 x 20 Grid

Figure 4.18 Geometry and Computational Grid for Shear Layer Mixing Problem

20 grid cells placed uniformly. The inner jet velocity was 53 m/s while the outer jet velocity was maintained at 9 m/s. The centerline variations in the mixture fraction are shown and compared to the measured data of Schefer and Dibble [28] in Figure 4.19. The comparison indicated good agreement upstream and satisfactory agreement downstream.

5. CODE DEMONSTRATION FOR FIRE PROBLEMS

5.1 Problem Selection

All verification cases, described in the previous section, have been of non-reactive flow nature. To demonstrate the code's capability for reactive flows, similar to those in typical fire problems, the following experimental investigations were considered as the potential source for a demonstration problem.

1. Cable burning experiments conducted by Factory Mutual Research Corporation (FMRC) under the sponsorship of the Electric Power Research Institute; EPRI Report NP-2660.
2. Tests for Twenty-foot Separation Criteria of NRC, conducted by Underwriters Laboratory in conjunction with Sandia National Laboratory; Report NUREG/CR-3192, SAND83-0306, 1983.
3. Tests for fire in compartments, conducted by the National Bureau of Standards; Report NBSIR-82-250, 1982.
4. Enclosure Environment Characterization testing for the Base Line Validation of Computer Fire Simulation Codes, tests conducted by FMRC, under the guidance of Sandia National Laboratories for the U.S. Nuclear Regulatory Commission; Report NUREG/CR-4681, SAND86-1296, 1987.

Of the above, the last series of tests have been found to be the most suitable because the tests were designed:

a) to simulate fire conditions of nuclear power plant enclosures; and
b) to provide data for the validation of fire modeling computer programs.

This test series included 22 tests, however, so far only limited data (for 3 tests) have been analyzed and reported in Reference 9.

In the following sections, the test cases will be described along with the numerical setup, and finally, the results will be presented, analyzed, and compared to the experimental results.

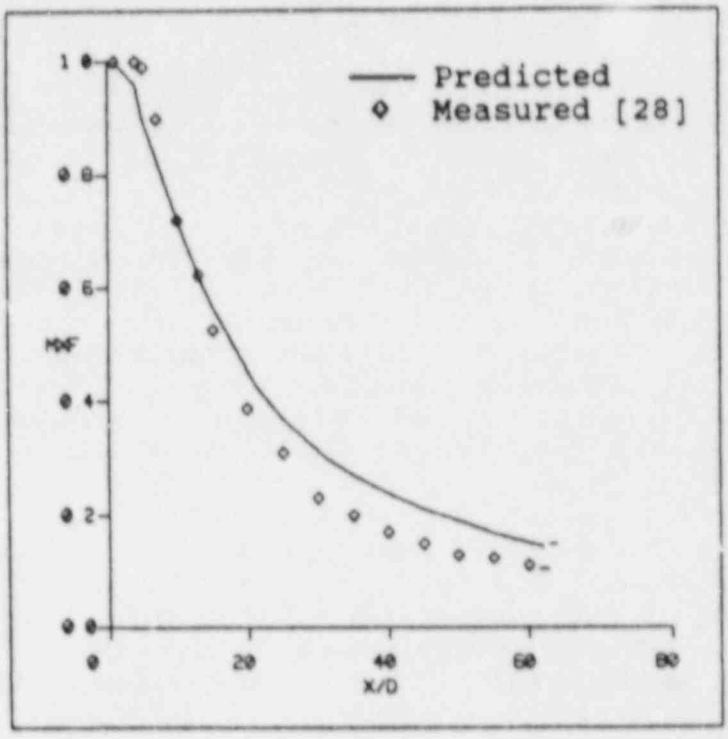

Figure 4.19 Predicted and Measured Mixture Fraction at the Centerline

5.2 Test Case Selected (FMRC/SNL/NRC)

Experimental Setup: The test enclosure has a size of sixty feet long by forty feet wide by twenty feet high (18 × 12 × 6 meters) as shown in Figure 5.1. A forced ventilation system with six inlet ports and one outlet port is used. The inlet ports extended down through the ceiling of the enclosure to a point four feet (1.2 meters) below the ceiling. These inlets were capped with standard, commercially available four-way air diffusers. The enclosure surfaces were instrumented at a number of locations for surface temperature, optical density, surface heat flux, etc. The fuel/fire sources utilized in the tests included gas burner fires, liquid pool fires, and simple solid fuel fires.

A total of eighteen Base Line Validation tests were conducted in the enclosure with no internal obstructions present, while another four Base Line Validation tests were conducted in a control room mock-up configuration of the test enclosure. Initial test results are available [9] for cases 4 and 5 of the non-internal obstruction cases, and case 21 which was a mock-up configuration test. Test case was selected as the base case for code validation. Cases 5 and 21 have also been considered for two-dimensional analysis with the fire code. These two-dimensional analyses will be presented later in this section; case 4 and its two-dimensional results are described first.

Case 4 utilized a gas burner fire source located near the middle of the room. The burner utilized was a 36-inch diameter sand burner. The gaseous fuel was forced to flow up through a base of loose sand filling the burner body. The nominal peak value of the heat release rates was measured to be 516 kW. The location of the fire along with the location of the instrumentation, for which results were presented, is shown in Figure 5.2. Figure 5.3 shows the heat release rate profile for the gas burner that was utilized in case 4. The numerical setup of case 4 is presented in the following section.

Grid and Boundary Conditions: Due to the symmetry of the geometry of the enclosure and the location of the fire (middle of the room), only half of the room was numerically modeled. A relatively coarse grid of 1980 control cells (9 in the horizontal x-direction, 11 in the vertical y-direction, and 20 in the other horizontal z-direction) was used. The grid was constructed in such a way that the instrumentation locations shown in Figure 5.2 would coincide the grid nodes. The ventilation inlets were placed in three cells located 1.2 meters below the ceiling. Each grid cell has an area of 0.46 × 0.46 m^2, which corresponds to that used in the experiment. The ducts that are used for air passage inside the room were modeled by blocked cells above the ventilation inlets. The three planes of the computational grid are shown in Figure 5.4.

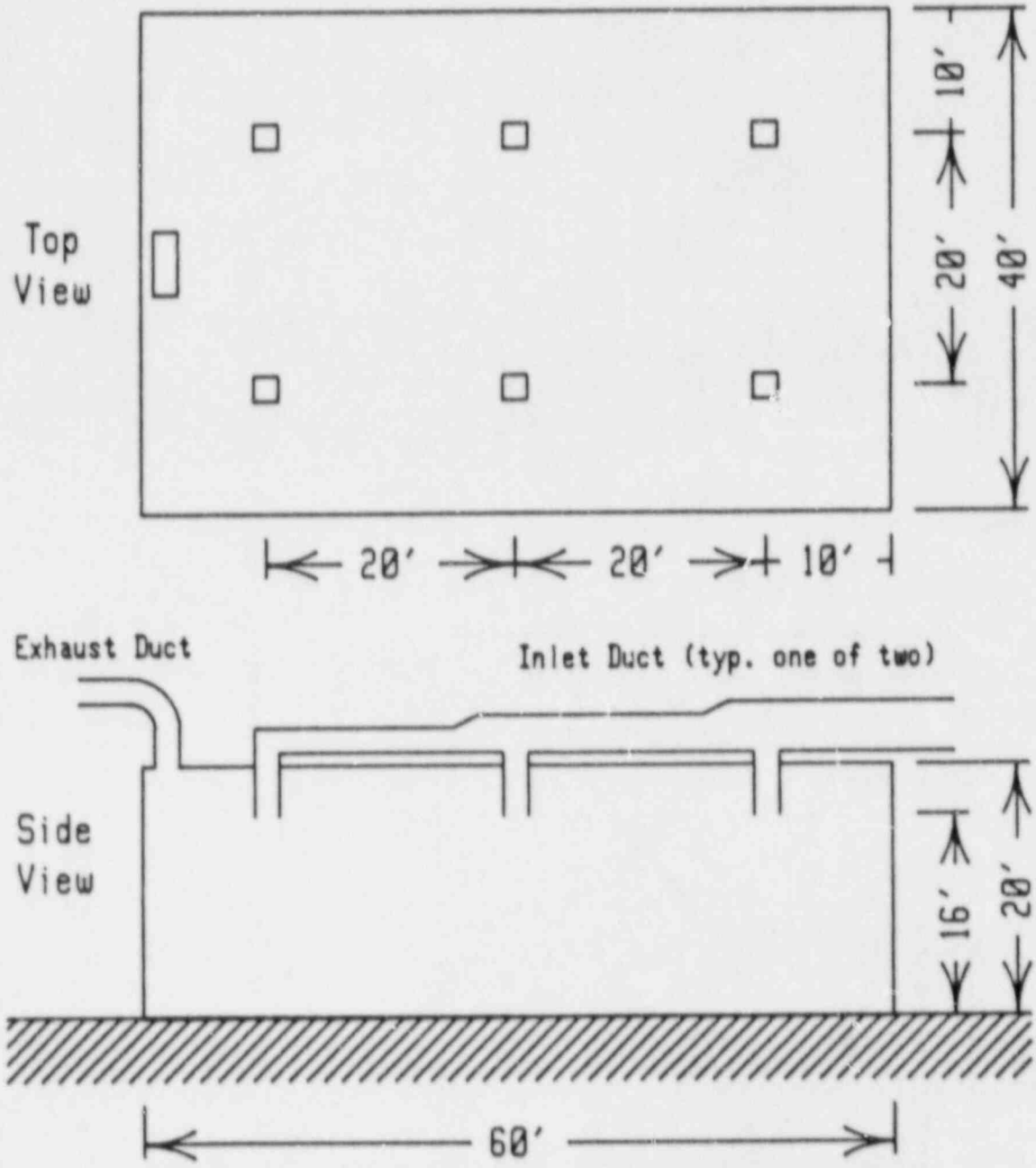

Figure 5.1 Enclosure Ventilation System of FMRC/SNL/NRC (1986/87) Tests

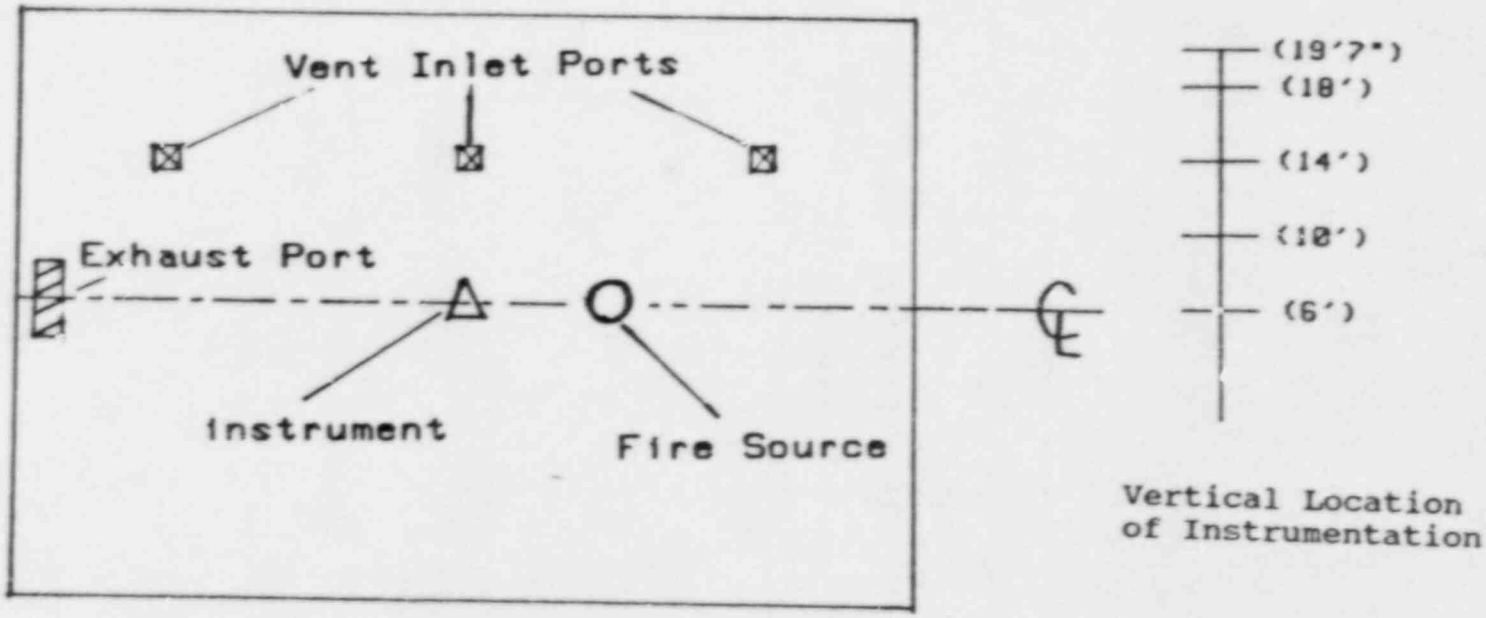

Note: Δ is the instrument location where the temperature measurements are available [8]

Figure 5.2 Location of Fire Source and Ventilation Inlet and Outlet Ports

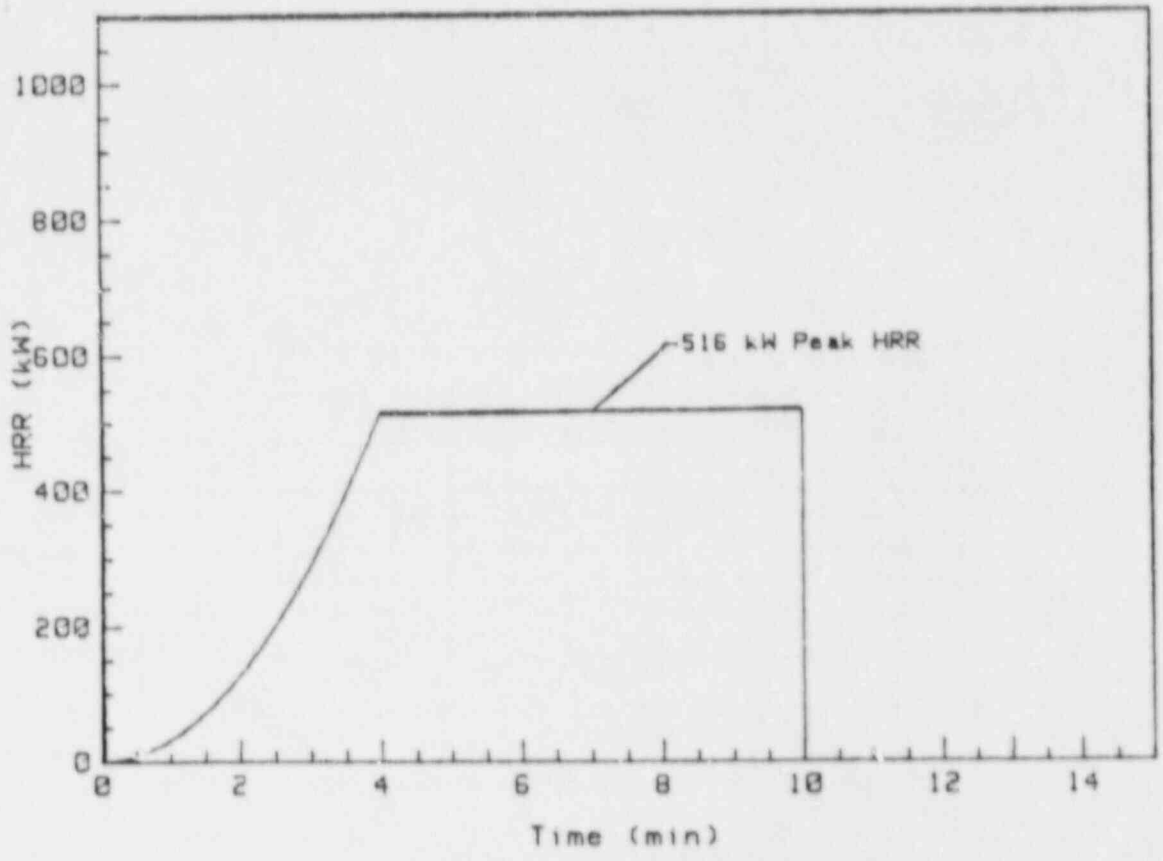

Figure 5.3 Measured and Simulated Heat Release Rate Profile

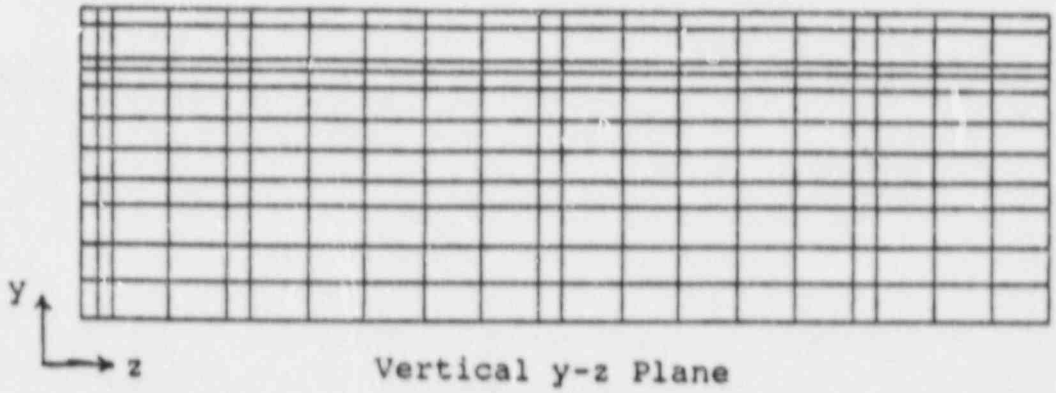

Vertical y-z Plane

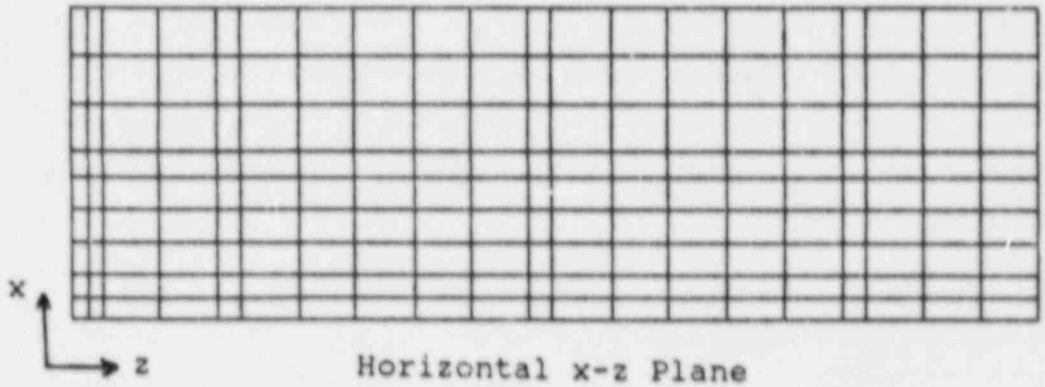

Horizontal x-z Plane

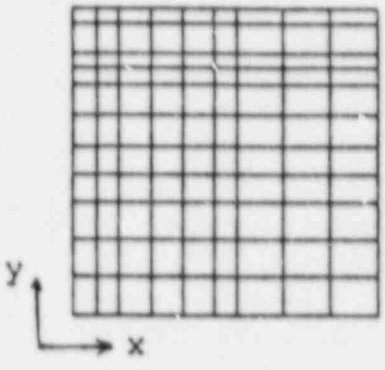

Vertical x-y Plane

Figure 5.4 Computational Grid Chosen for the Demonstration Calculation

The calculations were performed in two steps. First, steady-state (initial t=0, pre-fire) flow distribution is calculated with the following boundary conditions.

- Ventilation inlet mass flow rate of 0.076 kg/sec.
- Exhaust port zero relative pressure ($P_{exit} = 0$).
- Adiabatic walls.

Then the transient analysis is performed with the same boundary conditions and the fire source modeling. The transient combustion calculations were performed with the time intervals of Δt = 15 seconds.

Fire Source and Combustion Setup: In the experimental test case considered, the (non-premixed) gas propylene (C_3H_6) fuel was supplied through the sand burner. A diffusion flame resulted with a 36-inch base (burner diameter) extending upward to the ceiling of the enclosure. Experimental data for the heat release rate, HRR, shown in Figure 5.3, was used to compute the fuel mass flow rate from the following relation:

$$\dot{m} = \frac{HRR}{Q_L} \left[\frac{kg}{sec}\right] \qquad (30)$$

where $Q_L = 4.58 \cdot 10^7$ j/kg is the heat of combustion of propylene.

In the "growth-mode" heat release test, the resulting flow rate is proportional to the square of elapsed time from ignition to reach full intensity at four minutes. The peak value was maintained for the remaining six minutes, and then full cut off occured.

In the real diffusion flame environment the heat release rate will be distributed within the flame zone and will extend up to the ceiling of the enclosure. The spacial distribution of the heat release rate was unknown. It was decided, therefore, to use a simplified, global one-step finite-rate reaction model for the fuel combustion in the following form:

$$C_3H_6 + SO_2 \rightarrow 3CO_2 + 4H_2O \qquad (31)$$

Under real conditions, however, at relatively low temperatures, the combustion process may result in much slower heat release and several intermediate reactions, producing: C (soot), CO, C_2H_4, CH_2, H_2, etc. It should be indicated, therefore, that two types of inaccuracies will result from the assumed combustion model:

1. the overall heat release will be larger in the computational studies than in the experiments. As a result, the temperature levels may be over-predicted, and
2. single-step reaction will produce faster reaction rates

and may result in too large a heat release in the vicinity of the burner.

For the purpose of the present study, an Arrhenius reaction model was used to represent the reaction rate as:

$$R_{fu} = -\rho A M_{fu} \left(\frac{\rho\ m_{fu}}{M_{fu}}\right)^{\alpha} \left(\frac{\rho\ m_{ox}}{M_{ox}}\right)^{\beta} \exp\left(-\frac{E}{RT}\right) \qquad (32)$$

with rate constants $A = 1.10^{10}$, and $E/R = 18000$.

In the second phase of the project, a more adequate multi (two or four) step reaction model should be used as discussed in Section 2.3.

5.3 Results of 3-D Computations

Steady-State Results: The steady-state solution depicts the flow distribution under the normal forced ventilation conditions in a large, empty room with no fuel supply. Figure 5.5 shows velocity vectors in three planes of the computational domain. Figure 5.5a shows the velocity vectors at the vertical symmetry plane near the exit. As expected, the flow is strongest near the exit and shows an upward motion at the opposite side of the room, resulting from the third ventilation inlet near the end of the room. Figure 5.5b shows the velocity vectors in the mid-vertical plane where the ventilation inlets are located. It can be seen that the air exits from the ports and flows in all directions, resembling four-way diffuser outlets. The same phenomena is observed in Figure 5.5c, which shows the velocity vectors in the horizontal xz plane near the ventilation inlets.

Transient Results: As mentioned earlier, transient calculations were performed with fifteen second intervals (Δt=15 sec) for a total time of six minutes. Presented results from the transient analysis include velocity vectors and temperature contours at one minute intervals. Figure 5.6 shows the temperature contours in the vertical yz plane, where the fire is located. It is observed that as early as one minute, the hot temperature starts propagating in the room. For the first two minutes, a hot layer is observed near the ceiling. This hot layer propagates and descends into the room as time increases to five minutes. The fire phenomena is observed in all four plots, where the flame-shaped contours are observed above the fire. The temperature, as expected, increases with time due to the addition of heat, as shown in the profile in Figure 5.3. Figure 5.7 also shows the temperature contours in the vertical xy plane at the fire location. The same observations made earlier apply to these plots. The hot layer is clearly seen in the first three minutes. The layer descends into the room and the temperature near the fire increases to above 330°C at the four minute time.

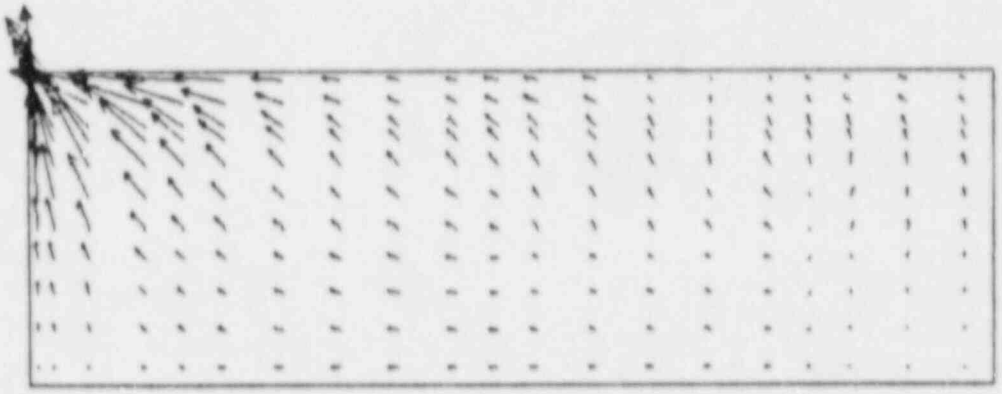

XZ Plane 1
Vmin = 0.00014 m/s
Vmax = 0.36 m/s

(a)

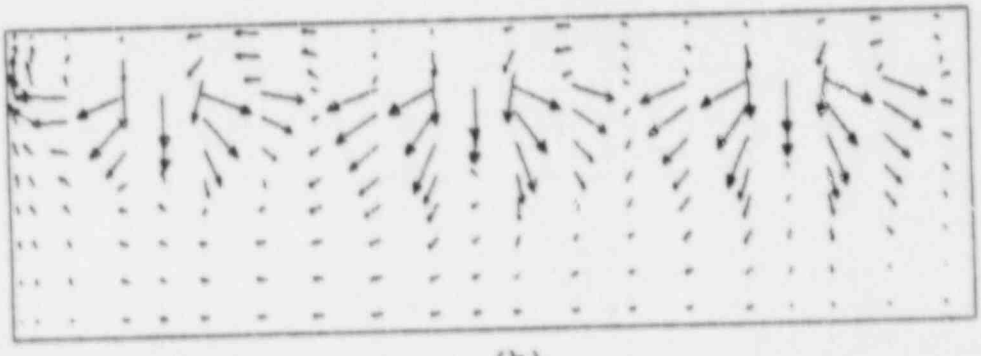

YZ Plane 6
Vmin = 0.0 m/s
Vmax = 0.057 m/s

(b)

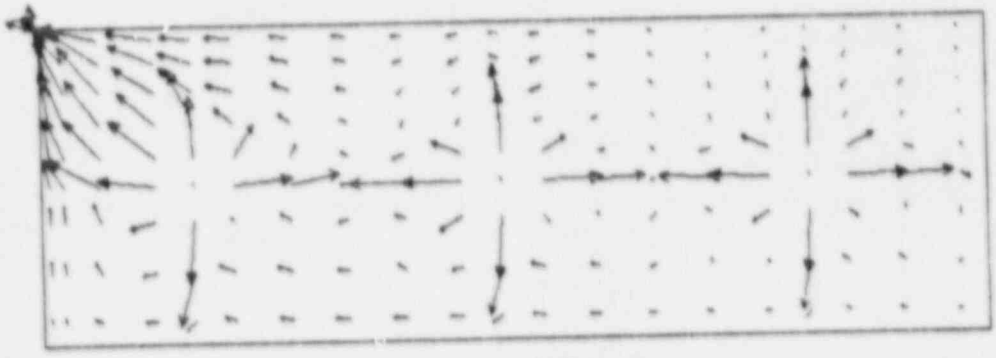

XZ Plane 8
Vmin = 0.0002 m/s
Vmax = 0.049 m/s

(c)

Figure 5.5 Calculated Velocity Distribution in the Test Room for Initial (Steady-State Pre-Fire) Condition

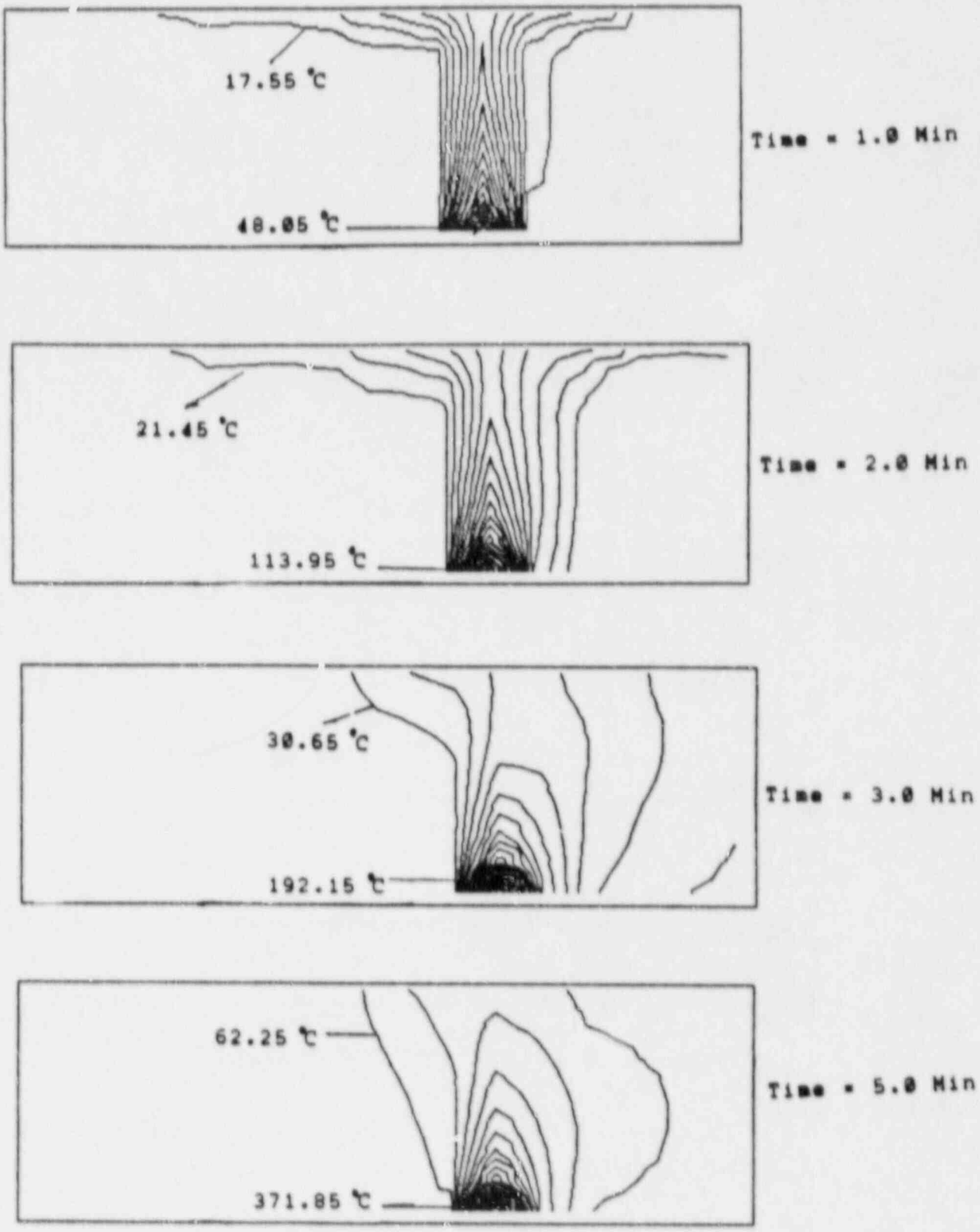

Figure 5.6 Temperature Contours at Near-Fire Vertical y-z Plane at t = 1, 2, 3, and 5 Minutes

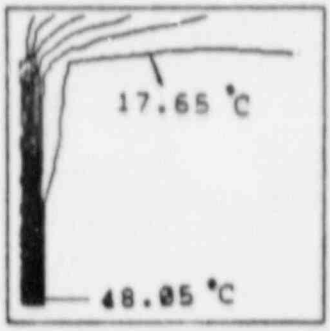

Time = 1.0 Min

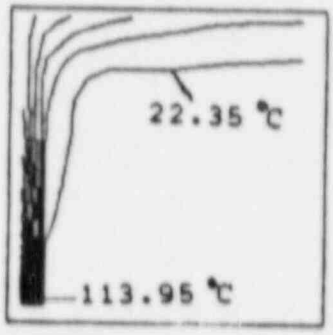

Time = 2.0 Min

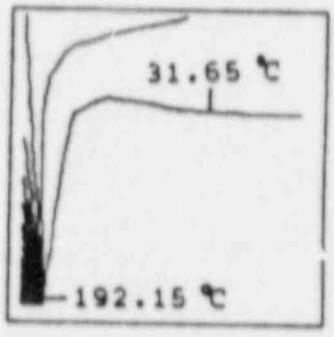

Time = 3.0 Min

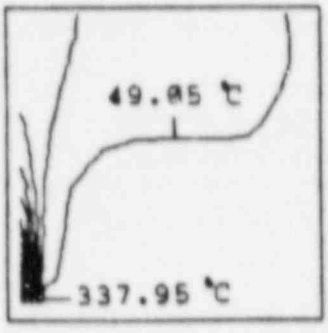

Time = 4.0 Min

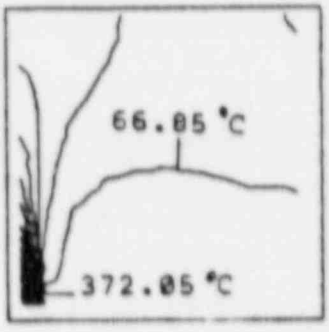

Time = 5.0 Min

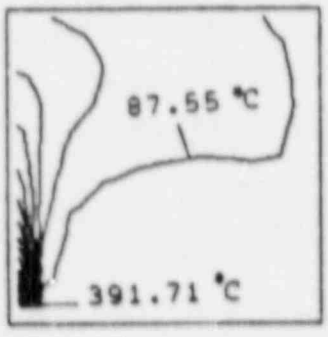

Time = 6.0 Min

Figure 5.7 Temperature Contours at Near-Fire Vertical x-y Plane at t= 1, 2, 3, 4, 5, and 6 Minutes

Figures 5.8, 5.9, and 5.10 show the velocity vectors in three vertical yz planes. Figure 5.8 shows the vectors in the first vertical yz plane near the fire. At one minute, it is observed that the air is entrained into the fire and accelerated vertically upward toward the ceiling, while the flow has no uniform or apparent pattern away from the fire. The same phenomena persists at the two minute time with a more uniform development of the flow. At four minutes, circulatory (eddy) motion is observed in different places of the room, with the biggest eddy located near the exit. The same phenomena is observed at five minutes.

Figure 5.9 shows the velocity vectors in the mid-vertical yz plane where the ventilation inlets are located. The same overall phenomena observed at the first vertical plane is observed here (viz: the circulatory motion or several flow eddies). The effect of the ventilation is observed in the first two minutes where the velocity is directed downward and away from the inlets with the circulation eddies being pushed toward the floor of the room. At four minutes, the effects of the ventilation disappears as the flow near the inlets is dominated by the circulation motions created by the fire and no motion from the inlet ports is observed.

Figure 5.10 shows the velocity vectors in the last vertical yz plane, at the end of the room. The circulation motion of the flow, which is a characteristic of fire flows, is still apparent and has a more pronounced shape at later times (four and five minutes).

Figure 5.11 presents a summary plot of the predicted and experimentally measured profiles at a vertical line located at the symmetry plane of the room close to the burner (the triangle in Figure 5.2). Results are compared for 2, 3, 4, and 5 minute intervals.

The overall tendency of the temperature pattern is similar in both computations and experimental measurements. At t=2 minutes after the ignition, the temperature profiles are very similar, with only 2°C over-prediction near the floor (6' level), and 8°C over-prediction near the ceiling (18' level). As the time increases, the profile shape remains similar, but the over-prediction of the temperature level becomes greater. The maximum over-prediction of temperature is observed at t=5 minutes, and is of the order of 30°C. Several factors contribute to the inaccuracy. Their relative importance is discussed on the following pages.

1. Grid Coarseness: With only one grid cell within the flame region (burner diameter equal to the cell size) the maximum flame temperature will be smeared within the cell. The real flame front temperatures may be as high as 1200°C, whereas cell averaged combustion zone temperatures are of the order of 370°C (Figure 5.6).

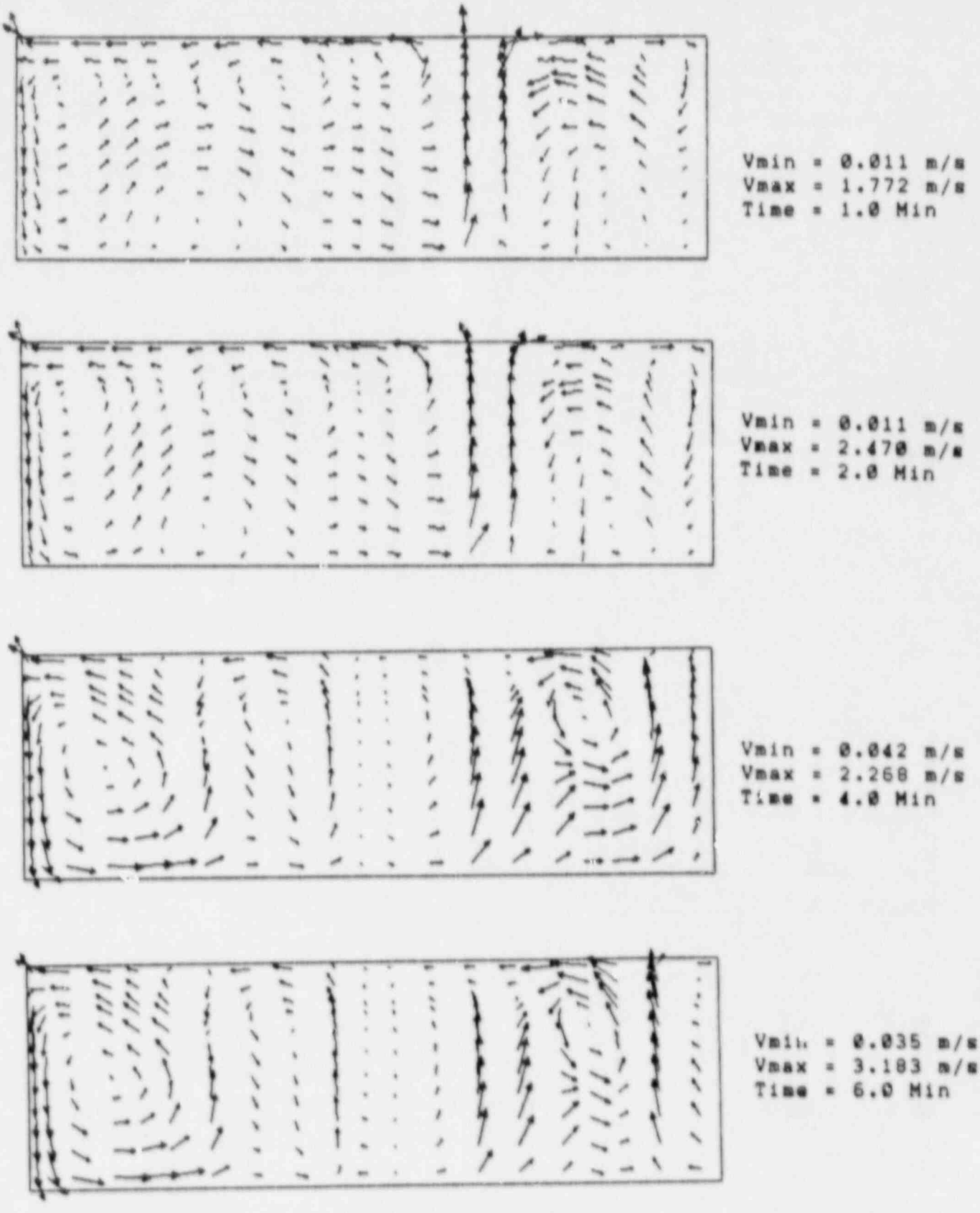

Figure 5.8 Velocity Contours at the First Vertical y-z Plane Near Ventilation Exit

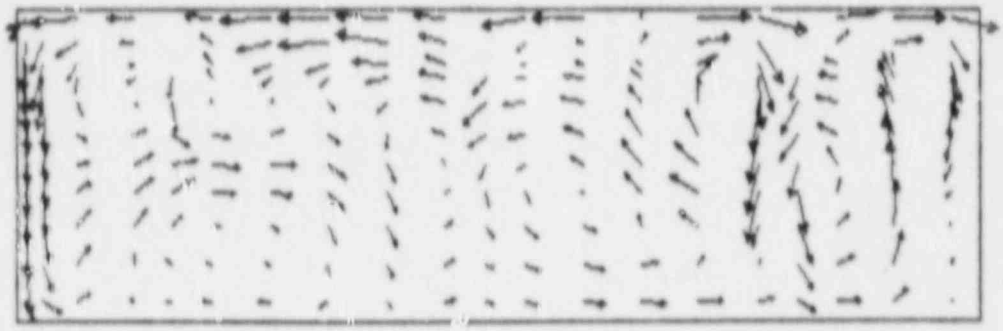

Vmin = 0.0 m/s
Vmax = 0.463 m/s
Time = 1.0 Min

Vmin = 0.000 m/s
Vmax = 0.794 m/s
Time = 2.0 Min

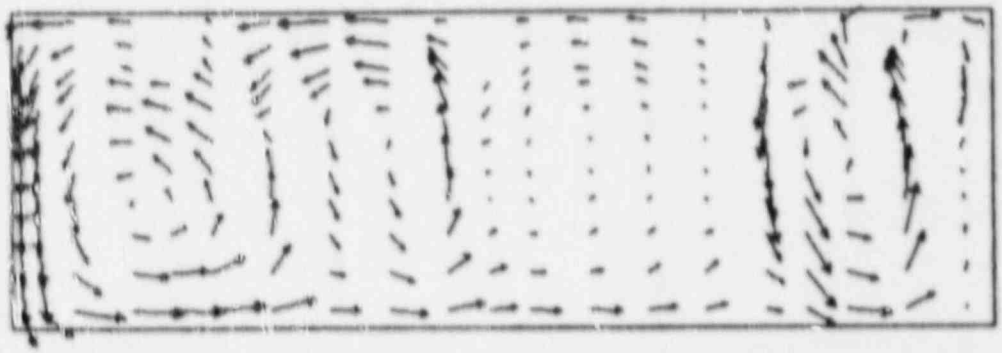

Vmin = 0.0 m/s
Vmax = 2.162 m/s
Time = 4.0 Min

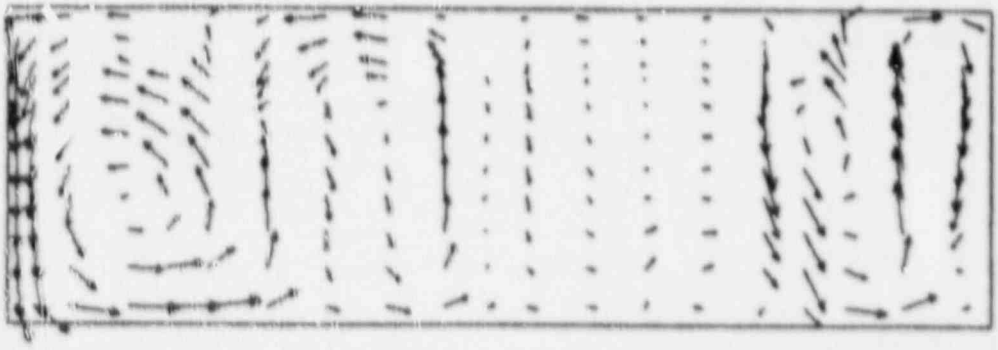

Vmin = 0.0 m/s
Vmax = 3.396 m/s
Time = 6.0 Min

Figure 5.9 Velocity Vectors at Mid-Vertical Plane
Near Ventilation Inlets (yz -

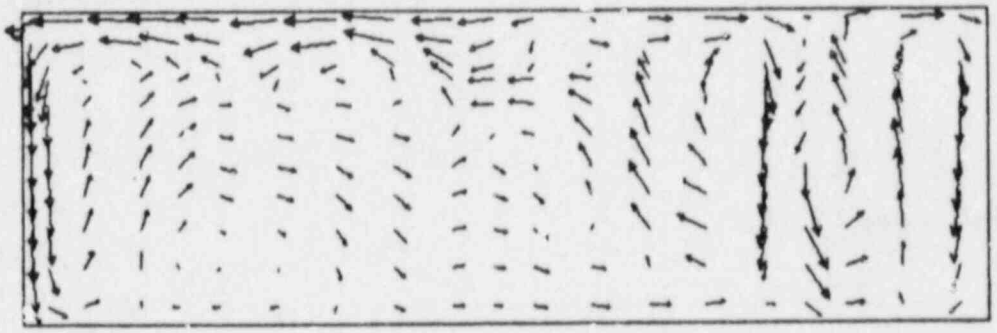

Vmin = 0.017 m/s
Vmax = 0.504 m/s
Time = 1.0 Min

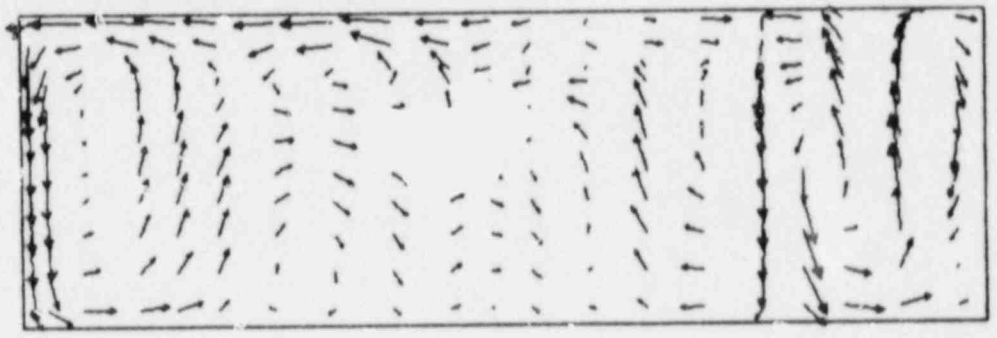

Vmin = 0.046 m/s
Vmax = 1.079 m/s
Time = 3.0 Min

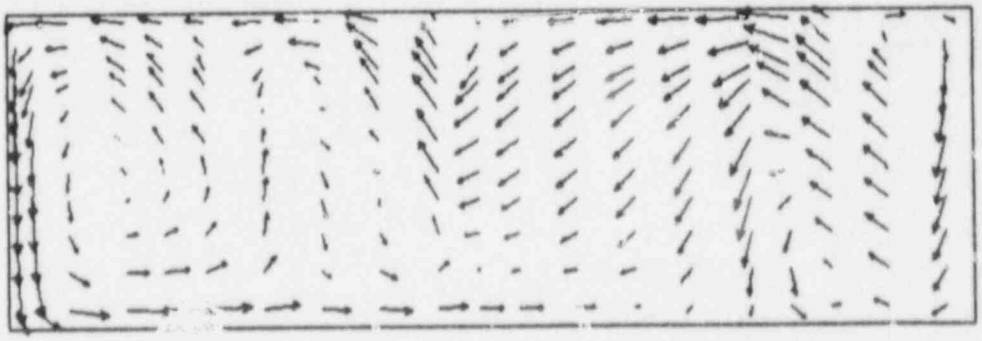

Vmin = 0.046 m/s
Vmax = 2.483 m/s
Time = 4.0 Min

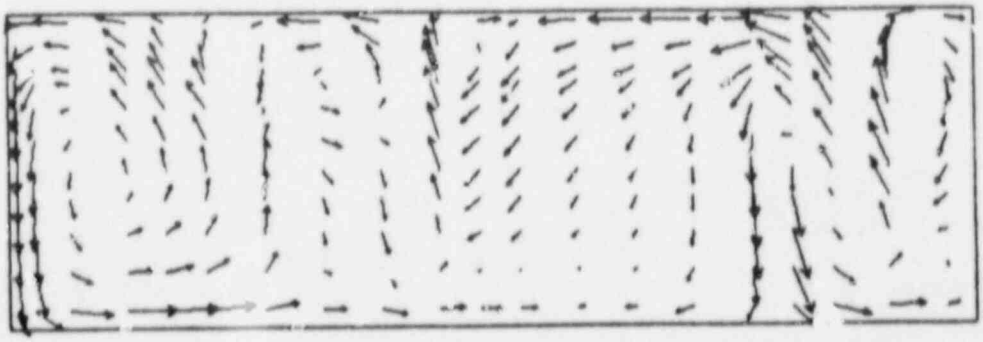

Vmin = .0453 m/s
Vmax = 3.673 m/s
Time = 6.0 Min

Figure 5.10 Velocity Vectors at the Last Vertical y-z Plane Near the Wall

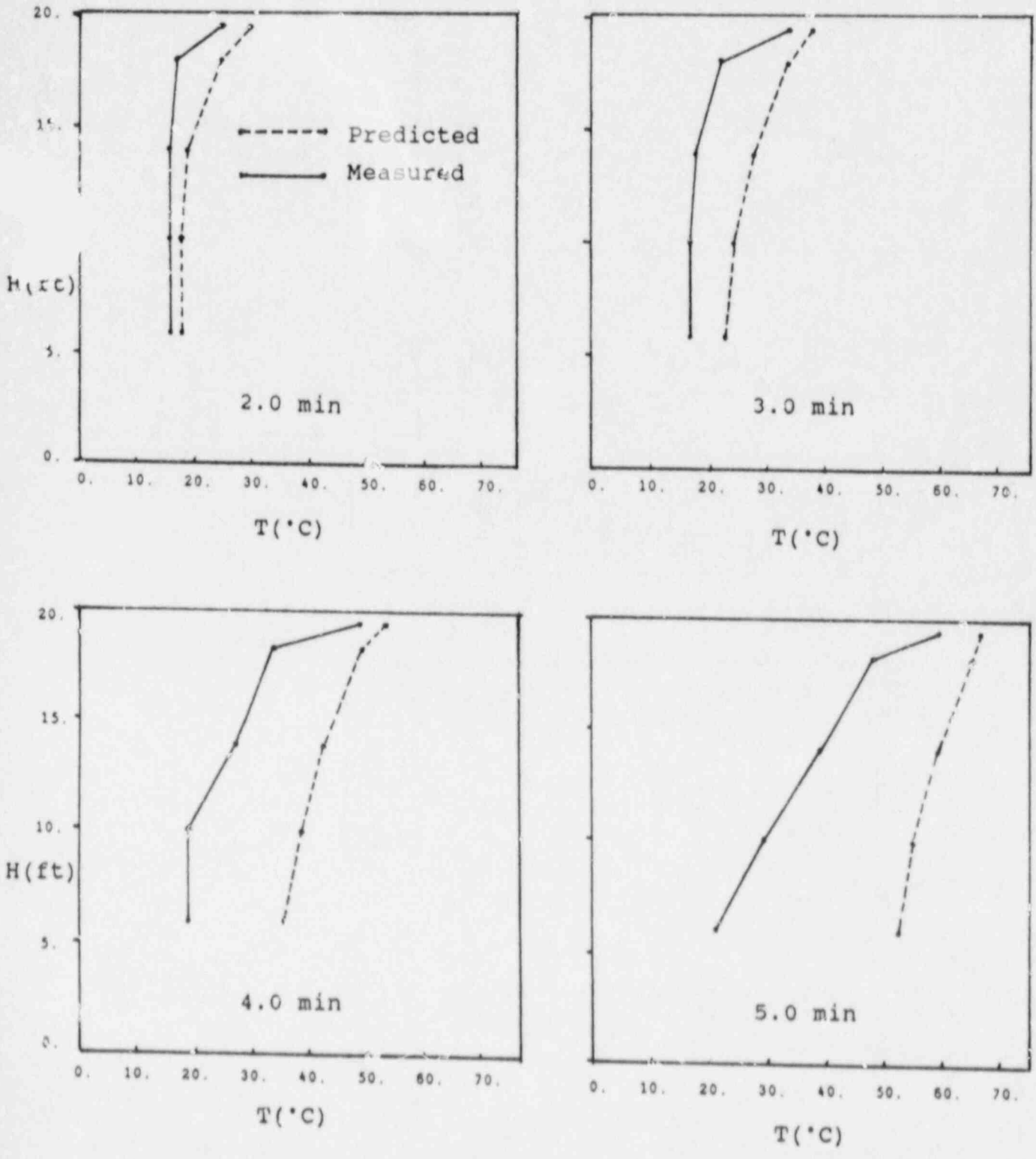

Figure 5.11 Comparison of Predicted Vertical Temperature Profiles with Experimental Data

The second inaccuracy will result from numerical diffusion in the region of high property gradients (flame zone). As a result, high temperatures will be predicted in the vicinity of the flame as well. This explains the largest over-prediction of temperatures at the six foot level, shown in Figure 5.11.

2. Combustion Model: As discussed earlier (section 2.3), the one-step reaction model will result in higher overall energy release and the release will take place mainly in the burner vicinity. This explains the higher temperature levels at the six foot elevation, and higher overall temperature levels. This inaccuracy can be significantly reduced by employing a multi-reaction model.

3. Wall Heat Transfer: Thermal radiation is the key mechanism of quick energy transfer between the high temperature flame and the solid walls (the flame-gas exchange is less important). The irradiated walls are then transferring the energy by convection to the boundary layer gases. As a result, significant energy is lost from the flame zone to all walls of the domain. Not accounting for radiation, in the flame vicinity, will contribute to higher predicted temperatures at the six foot level. In addition, the heat transfer between the irradiated walls and the nearby gas will contribute to a large vertical temperature gradient. This phenomena can be observed from experimental data. Lack of wall heat transfer (by convection and radiation) in our present demonstration calculations resulted in smoother temperature profiles, visible from Figure 5.11.

5.4 Investigatory 2-D Computations

To investigate the above-described contributing factors, and to further examine some of the basic code capabilities, a series of two-dimensional test cases were considered. The two-dimensional setup assumes only one plane in the x-direction while it maintains the same geometry in the vertical y-z plane. The boundary conditions used were the same as those used in the three-dimensional case. The inlet ports were placed at the same vertical and horizontal locations as in the three-dimensional problem. The ventilation rates were reduced by a factor of 6.1 proportional to the size of the room (viz: x-distance = 6.1 meters in 3-D; x-distance = 1 meter in 2-D) and were 0.0125 kg/sec. The fire source was maintained at the same locations, and the heat release rate was reduced by the same factor as the ventilation rates.

The reason for choosing two-dimensional instead of three-dimensional cases was the shorter computer time and fast turn-around

of two-dimensional computations. The cases selected include effects of:

- grid size;
- fire in a room with obstacles;
- sensitivity to ventilation inlet, velocity specifications, and size of exhaust port; and
- higher ventilation rates.

The following sections describe the cases used for two-dimensional analysis and present the obtained results.

Grid Size Sensitivity Study: In this study, two cases were considered. In the first case, the same grid as in the three-dimensional analysis, in the yz plane, was used. In the second case, the grid was refined to 35 x 19 grid cells, as shown in Figure 5.12b. A steady-state plus six minutes transient calculations were performed for both cases.

Results from the finer grid case are presented in Figures 5.13 and 5.14. Figure 5.13 shows the velocity vectors at steady-state and at four minutes of the transient. At the steady-state, the air exits from the inlet ports and flows in all directions with the overall motion being directed, as expected, toward the exit. At four minutes into the transient, the ventilation effects are overwhelmed by the buoyancy dominated flow, and the fire source is apparent. The phenomena of recirculation is observed as in the three-dimensional case. Figure 5.14 presents temperature contours at one and four minutes into the transient. Both plots show the hot layer near the ceiling. At four minutes, the hot layer descends toward the bottom of the room.

Results of the coarse grid calculation show the same phenomena. Figure 5.15 presents a comparison between coarse grid and finer grid results. For this comparison, the vertical temperature profiles, at the same location that was used for comparison with experimental results in the three-dimensional analysis, are plotted at 1, 2, 3, 4 5, and 6 minutes for both cases. It is observed that the hot layer, near the ceiling, is more pronounced in the fine grid case. Also, as expected, the temperature at the six foot level is lower when the finer grid is used. Both of those differences make the finer grid results relatively more agreeable with experimental data. Considerable further refinement is essential. Since the flow is truly three-dimensional, further grid-sensitivity studies should be three-dimensional, and should be conducted after the incorporation of improved physical models, in Phase II study.

Fire in Room with Obstacles: In this case, the same operational conditions were maintained along with the finer grid of the previous case. However, an obstacle was placed above the fire, as shown in Figure 5.16 by the shaded area.

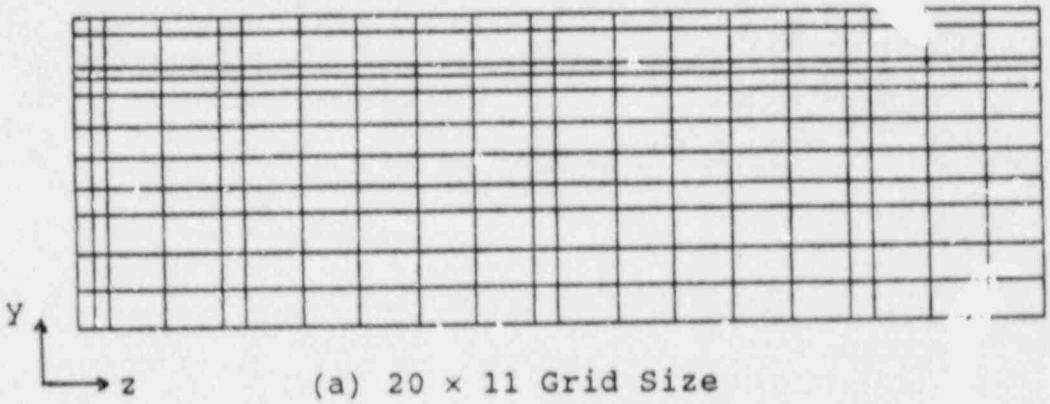

(a) 20 × 11 Grid Size

(b) 35 × 19 Grid Size

Figure 5.12 Computational Grids Used for Grid Sensitivity Study; (2-D Investigatory Problem)

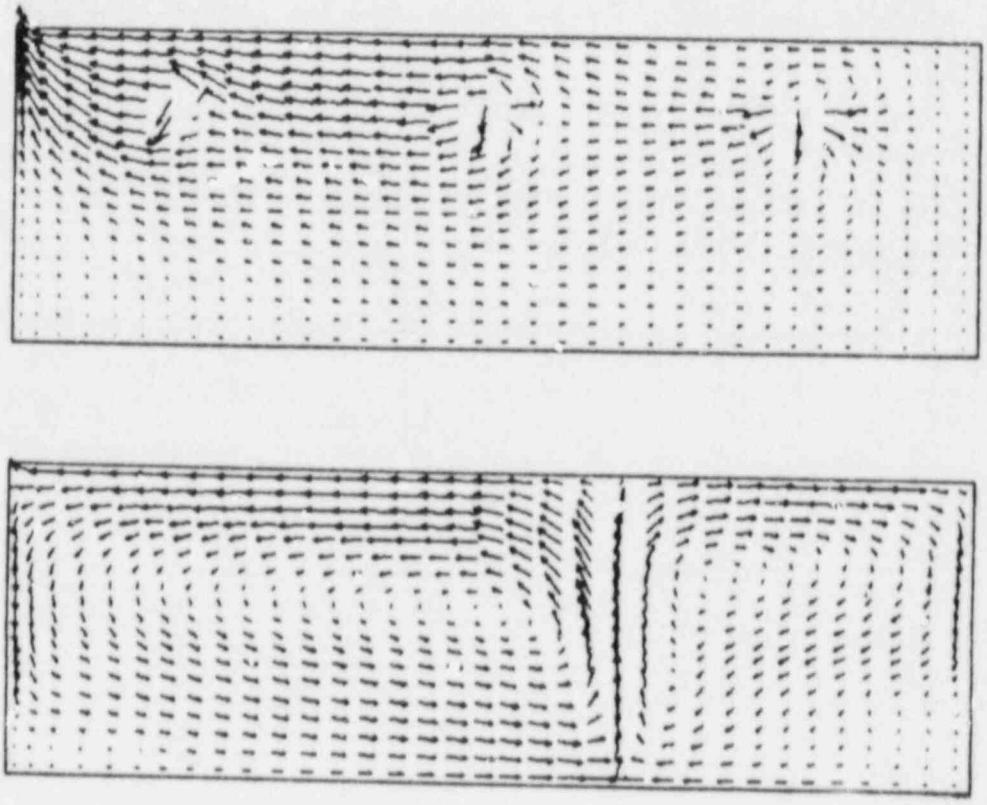

Figure 5.13 Velocity Vectors for Fine Grid

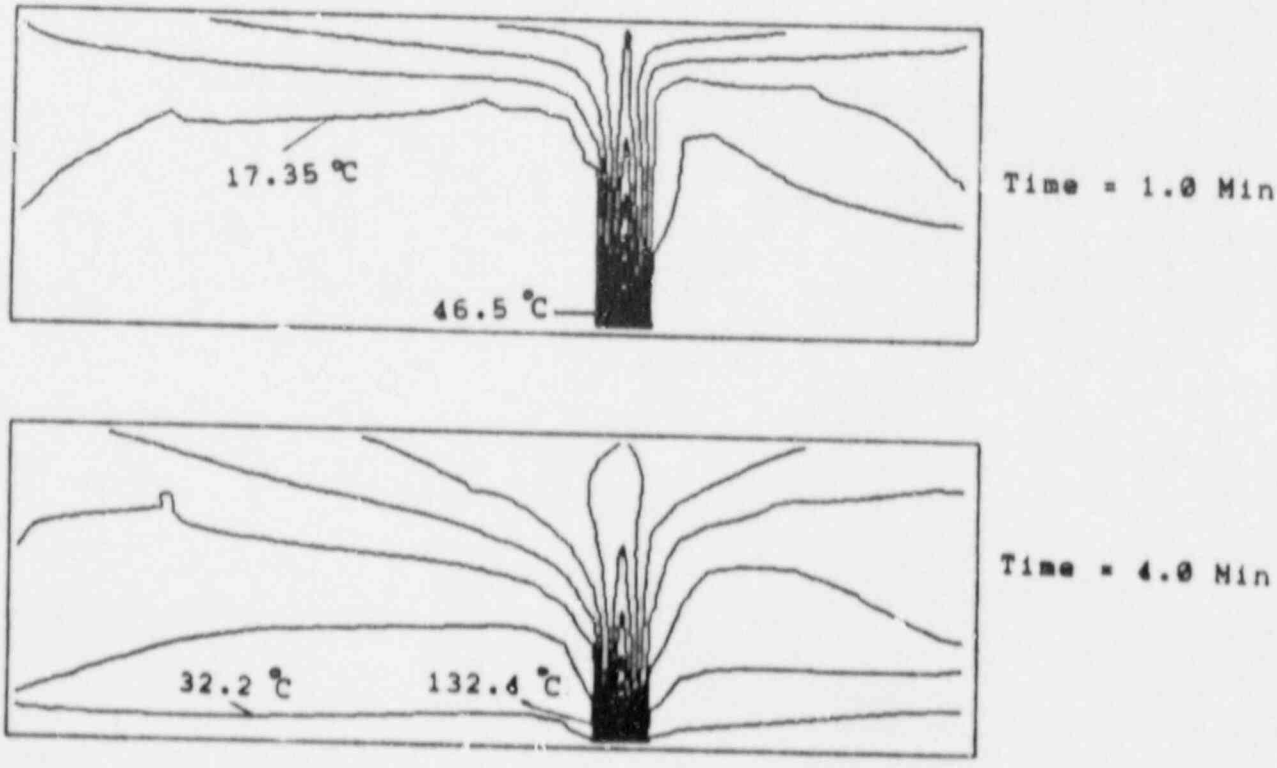

Figure 5.14 Temperature Contours for Fine Grid

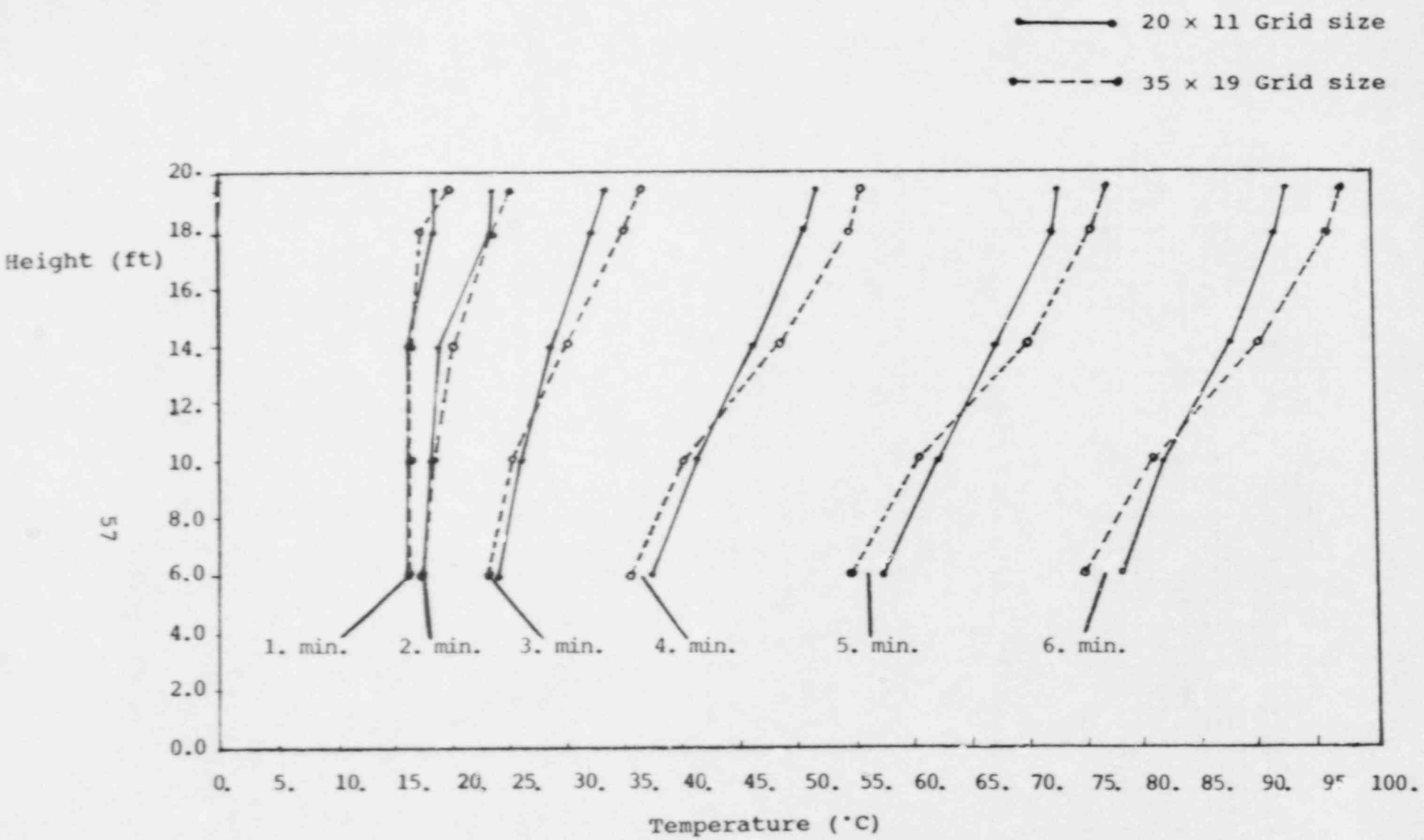

Figure 5.15 Vertical Temperature Profiles Near the Fire Source

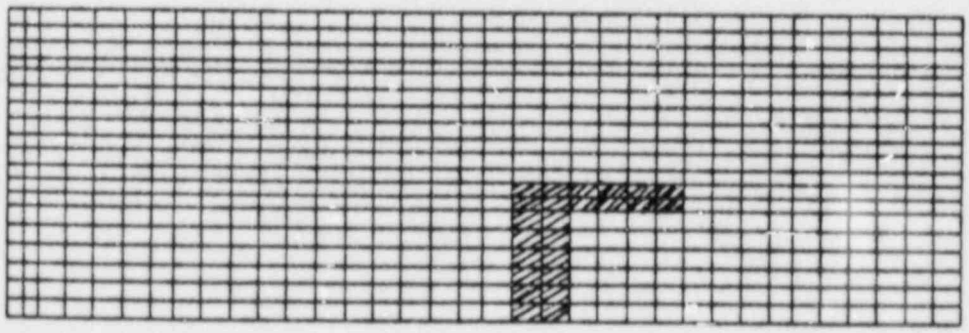

Figure 5.16 Fine Grid with Obstacles for Mock-Up 2-D Test Case

A steady-state and three-minute transient calculations were performed. Figure 5.17 shows the velocity vectors for the steady-state and at 1, 2, and 3 minutes of the transient. The velocity vectors in the steady-state are similar to those shown in the previous case, with a stronger flow above the blockage. After the fire starts, the flow pattern of the air changes dramatically, where the ventilation inlet port influence is not observed any more, even at one minute time. However, two recirculation regions are formed, one below the blockage and the other above the blockage, and extend up to the exit. The cold air is entrained into the fire, then accelerated from under the blockage. Some of this hot air escapes toward the ceiling, because of its lower density, creating a big recirculation motion in the room.

Figure 5.18 shows the temperature contours at the 1, 2, and 3 minute times of the transient. At one minute, the temperature contours resemble a flame in the middle of the room. However, at two and three minutes, the flame develops and a hot layer is formed near the ceiling.

Effects of a Wider Exhaust Outlet: The results of the above-described case showed a large recirculation zone under the exit. To examine whether or not this recirculation region is influenced by the size of the exhaust port, it was decided to model the same case with a wider outlet (exit area almost doubled). Figure 5.19 shows the velocity vectors for this case. At the steady-state, the same overall pattern of the flow is observed and the effect of the wider outlet is apparent by four velocity vectors which are directed outward near the exit. Also, the maximum velocity is almost halved when the exit is widened. At one and two minutes, the effect of the size of the exit diminished as the flow pattern resembles that of the narrower exit (Figure 5.17). As before, the wide recirculation zone persists.

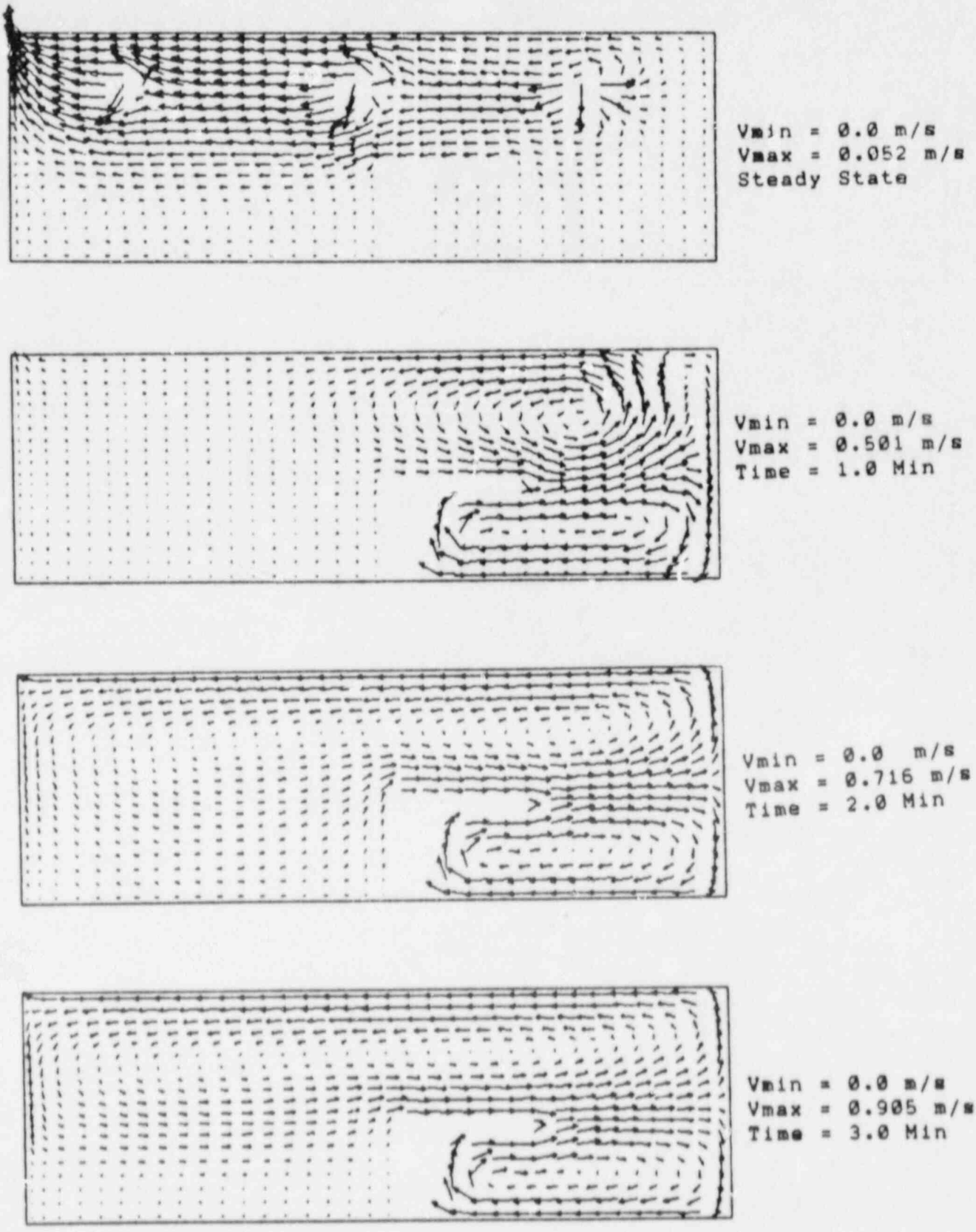

Figure 5.17 Predicted Velocity Vectors for Fine Grid with Obstacles

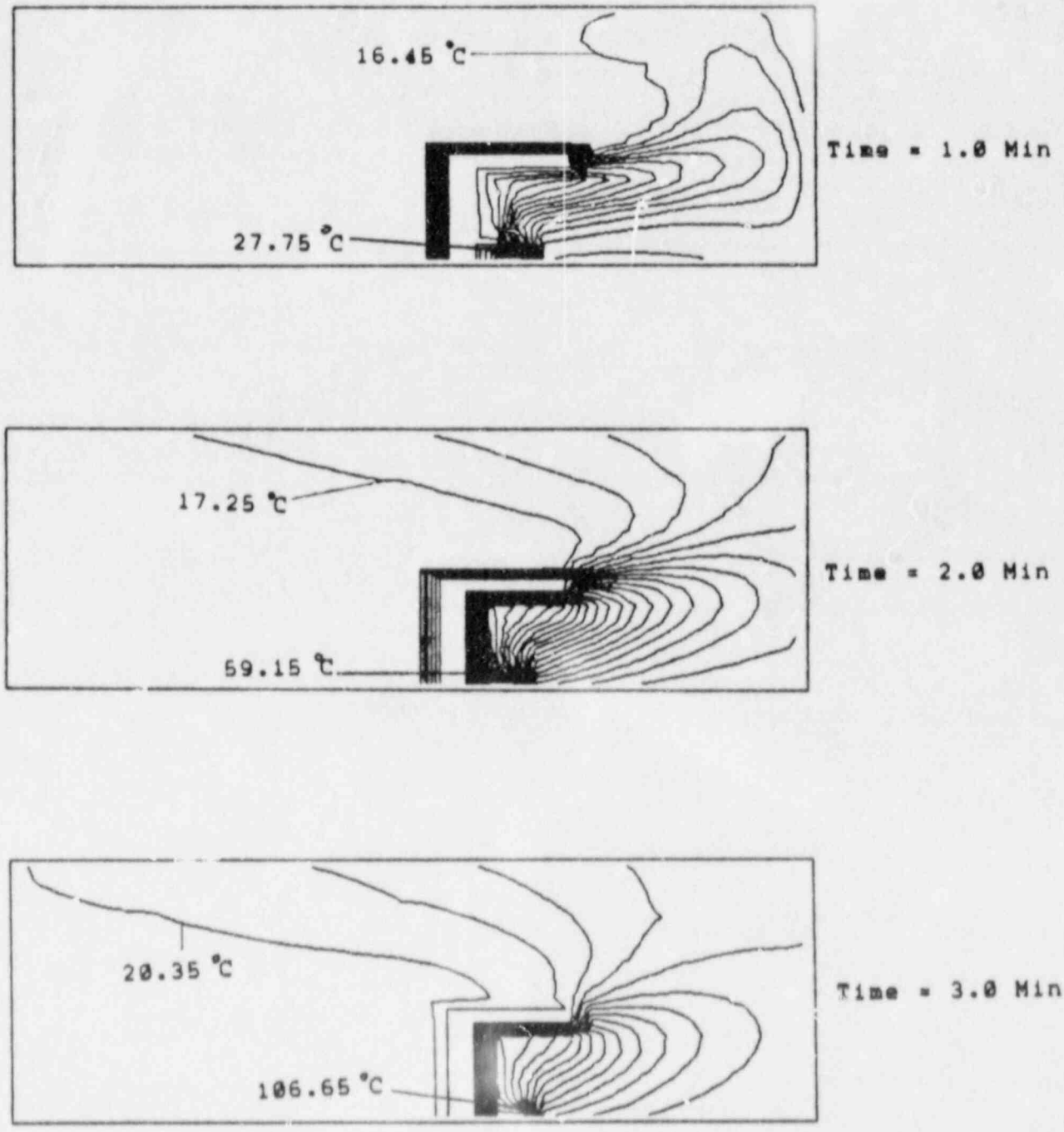

Figure 5.18 Temperature Contours for Flow with Obstacles

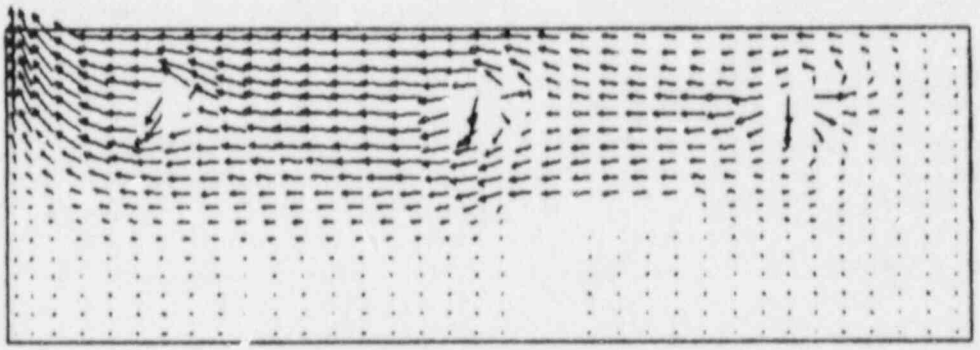

Vmin = 0.0 m/s
Vmax = 0.022 m/s
Steady State

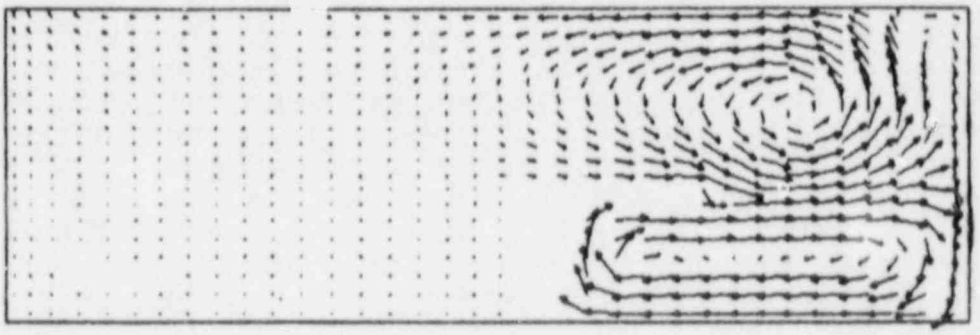

Vmin = 0.0 m/s
Vmax = 0.497 m/s
Time = 1.0 Min

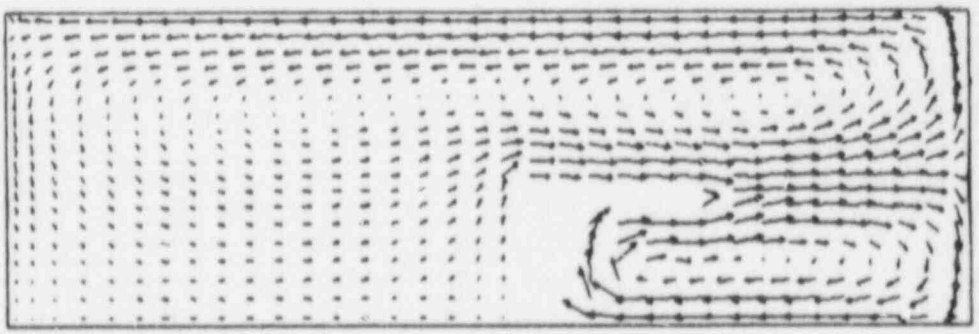

Vmin = 0.0 m/s
Vmax = 0.717 m/s
Time = 2.0 Min

Figure 5.19 Predicted Velocity Distribution for a Wider Ventilation Outlet

Effects of Simulating Ventilation Air with Finite Momentum: In the above cases, the ventilation air at the inlet ports was simulated as a mass source, and zero momentum source, i.e. it distributed equally in all directions. In the present case, the air was forced to flow vertically downward with finite momentum (no four-way diffuser effect). A steady-state plus three minutes of the transient calculation were made. Figure 5.20 shows the velocity vectors for the steady-state, one minute and two minutes time into the transient. At the steady-state, the only difference in flow pattern, from that in Figure 5.17, is observed near the inlet ports where strong or downward flow motion is seen. After the fire starts, at one and three minutes, the effects of the ventilation are insignificant and the overall pattern resembles that of Figure 5.17.

Effects of Increased Ventilation Flow Rate: To observe the effect of the increase in the ventilation rate, another two-dimensional test case was set up using ten times higher ventilation rate. This increased ventilation rate corresponds to that used in case 5 of the experiment [9]. The finer grid along with four-way diffuser effects were used in this case. A steady-state and three-minute transient simulations were performed. Figure 5.21 shows the velocity vectors for steady-state and at 1, 2, and 3 minutes of the transient. The overall pattern of the flow is similar to that of the lower inlet rates shown earlier in Figure 5.17. However, the ventilation inlets are still observed at one and two minutes into the transient. Figure 5.22 shows the temperature contours at 1, 2, and 3 minutes of the transient. At two minutes after the fire starts, the level of the contours is, as expected, somewhat lower when the ventilation rate is higher.

6. CONCLUSIONS AND RECOMMENDATIONS

6.1 Achievements of Phase I Study

A fire modeling computer code has been developed by using well-tested solution techniques. As a result, within the short (six month) period of the present study, it has been possible to develop, verify and demonstrate basic capabilities of the code. The results presented in Sections 4 and 5 clearly establish the feasibility of consolidating relevant techniques into a fire code, which can be widely used by various organizations concerned with the efficient and safe operation of nuclear power plants.

6.2 Recommendations for Phase II Work

The work completed in Phase I has clearly established the feasibility of an advanced state-of-the-art fire simulation code. To convert this code into a **reliable and usable** code (i.e. fully validated and well-documented code), the following work items are recommended for SBIR Phase II study.

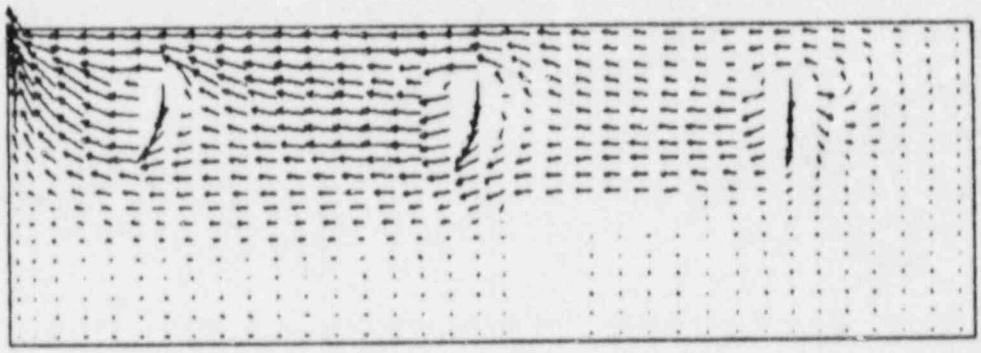

Vmin = 0.0 m/s
Vmax = 0.021 m/s
Steady State

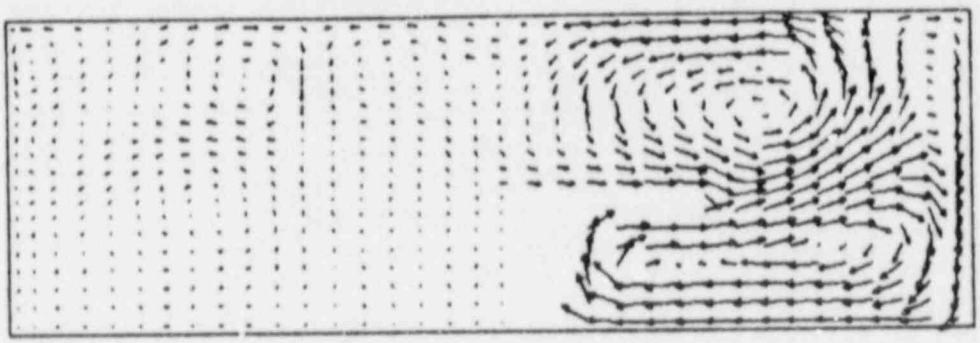

Vmin = 0.0 m/s
Vmax = 0.528 m/s
Time = 1.0 Min

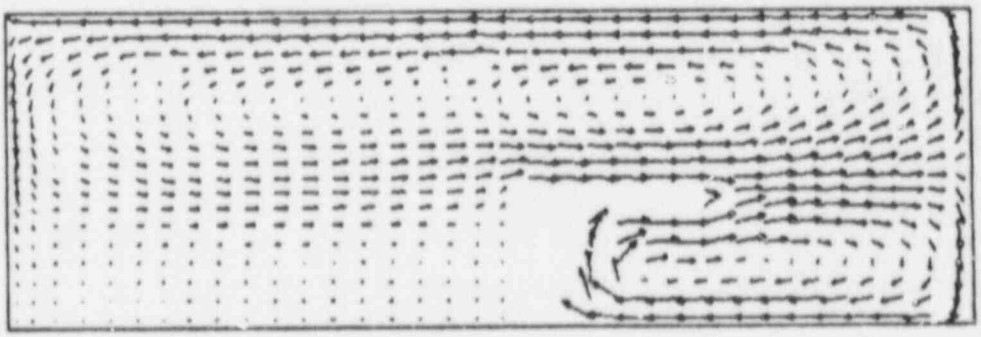

Vmin = 0.0 m/s
Vmax = 0.907 m/s
Time = 3.0 MIN

Figure 5.20 Velocity Distribution for Ventilations with No Diffusers

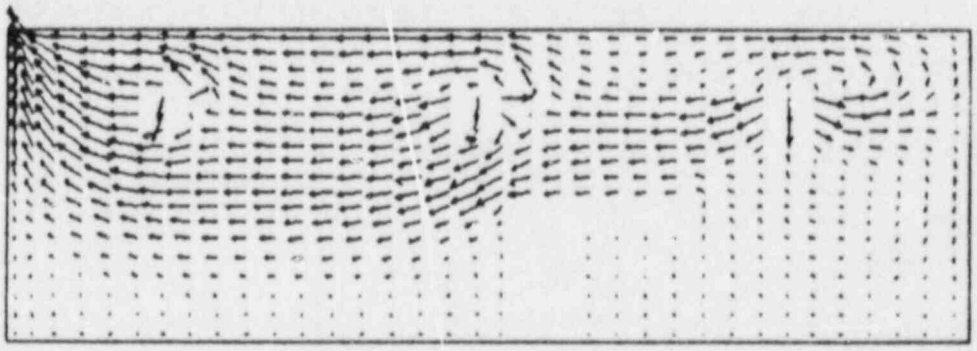

Vmin = 0.0 m/s
Vmax = 0.529 m/s
Steady State

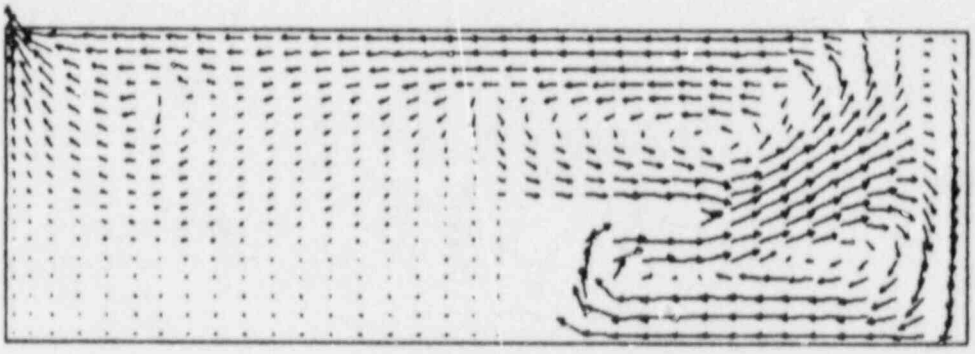

Vmin = 0.0 m/s
Vmax = 0.542 m/s
Time = 1.0 Min

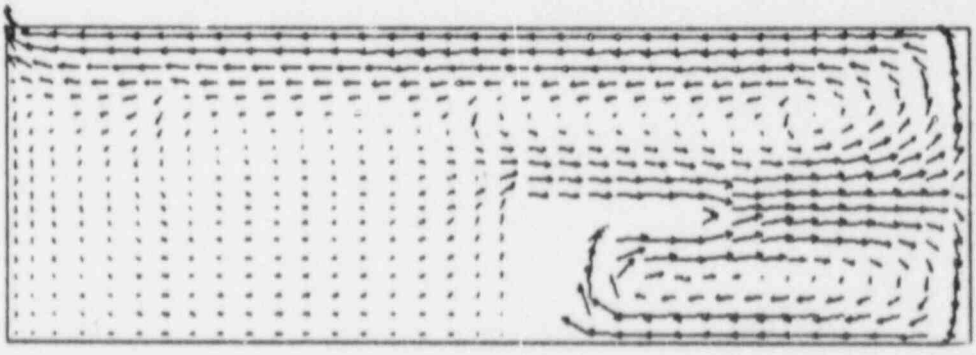

Vmin = 0.0 m/s
Vmax = 0.716 m/s
Time = 2.0 Min

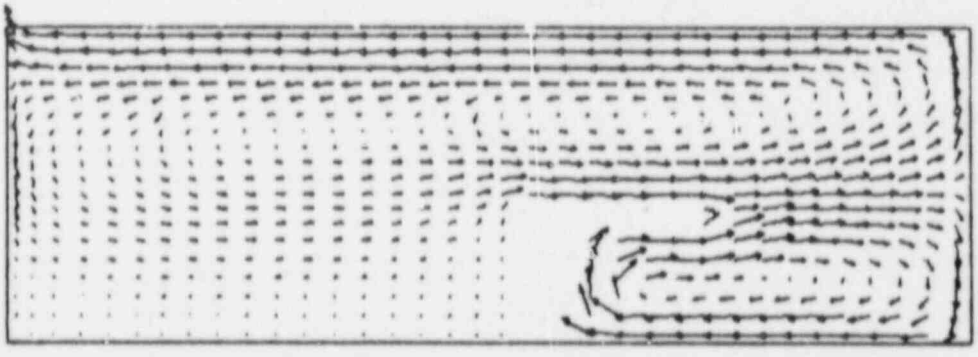

Vmin = 0.0 m/s
Vmax = 0.907 m/s
Time = 3.0 Min

Figure 5.21 Calculated Velocity Vectors for Higher Ventilation Inlet Flow Rates

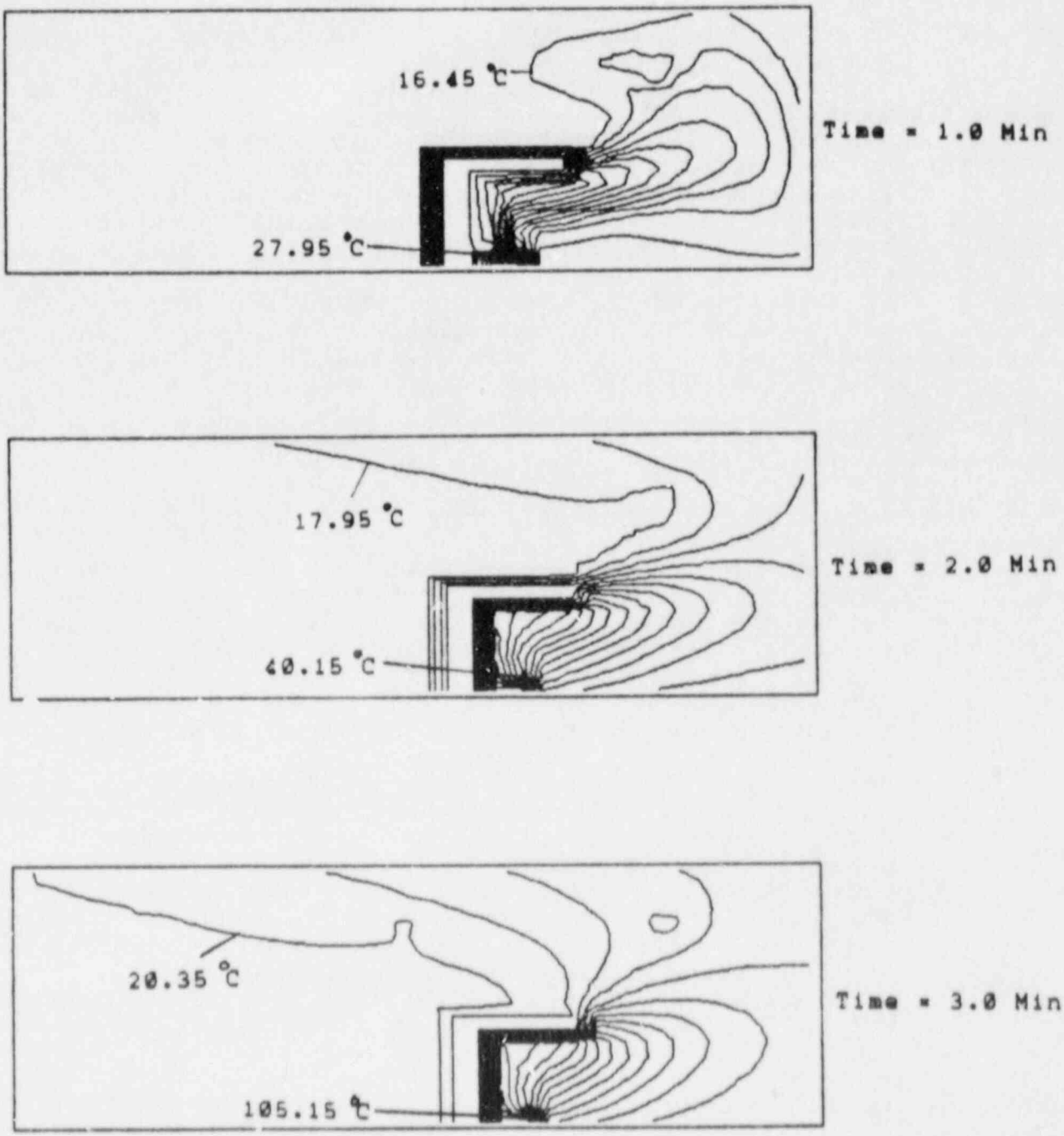

Figure 5.22 Temperature Contours for Higher Ventilation Inlet Flow Rates

1. Completion and testing of the physical models (described in Section 1.3).
2. Systematic parametric studies to establish the sensitivity of results to computational mesh, and various physical models.
3. Validation of the code against several (at least six) test cases of the 1986-87 NRC/SNL/FMRC experiments. If necessary, additional data from earlier tests (published by SNL, NBS, EPRI, FRS (UK), etc.) should also be used.
4. Finalization of the code, with emphasis on the ease-of-use, modularity, and portability.
5. Documentation of the code (including all assumptions, theoretical models, code structure and user's guide).

A detailed work plan with time and cost estimates will be submitted to NRC in the SBIR Phase II proposal.

6.3 Recommendations for Phase III Work

After the satisfactory completion of Phase II work, to effectively utilize and disseminate the developed code, the following three activities are recommended to be carried out with commercial and/or non-SBIR government funds.

1. Incorporation of selected data bank, i.e. physical properties and models for typical fire sources pertinent to nuclear power plants.
2. Enhancement of graphical display of results (improved color graphics and animation of results) so that the time evolution of the fire environments can be presented (and recorded) in the form of movies and/or video cassettes. Such movie (real-time) presentations are very helpful in general comprehension of complex flow developments, and can be very useful in assessing various safety aspects such as evacuation time.
3. Development of technical training and user support material, and a provision for code maintenance and necessary enhancements.

For items 1 and 2 above, necessary support will be sought from commercial organizations such as: Factory Mutual, Ove Arup & Partners, and IBM. In the past, these organizations have shown positive inclinations, however, due to the uncertainty and delay in NRC's request for 1988 SBIR proposals, no formal agreements have been established.

For item 3 above, CFDRC plans to provide the necessary support from its internal funds.

7. REFERENCES

1. Cline, D.D., Von Riesemann, W.A., and Chavez, J.M., "Investigation of Twenty-Foot Separation Distance as a Fire Protection Method as Specified in 10CFR50, Appendix R," NUREG/CR-3192, SAND83-0306, October 1983.
2. Singhal, A.K. and Tam, L.T., "Three-Dimensional Transient Fire Environment Predictions," reported in the PRC/NASA Report; "Solid Rocket Motor/Vehicle Assembly Building Inadvertent Ignition Effects Study," NASA KSC-DF-441, September 1981.
3. Boccio, J.L., Usher, J.L., Singhal, A.K., and Tam, L.T., "The Use of a Field Model to Analyze Probable Fire Environments Encountered within the Complex Geometries of Nuclear Power Plants," paper presented at the 23rd National Heat Transfer Conference, Denver, Colorado, August 1985, published in *Fire and Combustion Systems*, HTD vol. 45, pp. 159-166.
4. Usher, J.L., Boccio, J.L., Singhal, A.K., and Tam, L.T., "Fire Environment Determination in the LaSalle NPP Control Room," paper presented at the International ANS/ENS Topical Meeting on Operability of Nuclear Power Systems in Normal and Adverse Environments in Albuquerque, New Mexico, September 29 - October 3, 1986.
5. Markatos, N.C., Malin, M.R., and Cox, G., "Mathematical Modeling of Buoyancy-Induced Smoke Flow in Enclosures," *Int. J. Heat Mass Transfer*, vol. 25, no. 1, pp. 63-75, 1982.
6. Markatos, N.C. and Cox, G., "Turbulent Buoyant Heat Transfer in Enclosures Containing a Fire Source," Seventh International Heat Transfer Conference, Munchen, 6, p. 373, 1982.
7. Yang, K.T., Kelleher, M., Yang, H.Q., and Raycraft, J., "Field Modeling of Fire and Smoke Spread in Confined Spaces,"; Technical Report, Department of Aerospace and Mechanical Engineering, Unversity of Notre Dame, 1987, paper under preparation.
8. Boccio, J.L. and Usher, J.L., "The Use of a Field Model to Assess Fire Behavior in Complex Nuclear Power Plant Enclosures: Present Capabilities and Future Prospects," NUREG/CR-4479, BNL-NUREG-51948, December 1985.
9. Nowlen, S.P., "Enclosure Environment Characterization Testing for the Base Line Validation of Computer Fire Simulation Codes," prepared by Sandia National Laboratories for the U.S. Nuclear Regulatory Commission, NUREG/CR-4681, SAND86-1296, 1987.
10. Launder, B.E. and Spalding, D.B., *Mathematical Models of Turbulence*, Academic Press, London, 1972.
11. Kim, S.W. and Chen, C.P. "A Multiple-Time-Scale Turbulence Model Based on Variable Partitioning of Turbulent Kinetic Energy Spectrum," AIAA-88-1771, 1988.
12. Spalding, D.B., "Concentraton Fluctuations in a Round Turbulent Free Jet," *Chem. Eng. Sci.*, vol. 26, pp. 95-107, 1971.

13. Magnussen, B.F. and Hjertager, B.M., "On Mathematical Modeling of Turbulent Combustion with Special Emphasis on Soot Formation and Combustion," 16th Symposium (International) on Combustion, The Combustion Institute, pp. 719-729, 1976.
14. Hautman, D.J., Dryer, F.L., Shug, K.P., and Glassman, I., "Multistep Overall Kinetic Mechanism for the Oxidation of Hydrocarbons," *Comb. Science and Tech.*, vol. 25, nos. 5, 6, 1981.
15. Chandrasekhar, S., "Radiative Transfer," Dover Publications, New York, 1960.
16. Lockwood, F.C. and Shah, N.G., "A New Radiation Solution Method for Incorporation in General Combustion Prediction Procedures," Eighteenth Symposium (International) on Combustion, The Combustion Institute, Pittsburgh, Pennsylvania, 1981.
17. Lockwood, F.C. and Spalding, D.B., "Predictions of a Turbulent Reacting Duct Flow with Significant Radiation," Thermodynamic Session, Proc. Colloques d'Evian de la Societe Francaise de Physique, May 1981.
18. Patankar, S.V. and Spalding, D.B., "A Calculation Procedure for Heat, Mass and Momentum Transfer in Three-Dimensional Parabolic Flows," *International Journal of Heat and Mass Transfer*, vol. 15, pp. 1787-1806, Pergamon Press, 1972.
19. Patankar, S.V., "Numerical Heat Transfer and Fluid Flow," McGraw Hill, 1980.
20. Van Doormaal, J.P. and Raithby, G.D., "Enhancement of the SIMPLE Method for Predicting Incompressible Fluid Flows," *Numerical Heat Transfer*, vol. 7, pp. 147-163, 1984.
21. Przekwas, A.J., "Whole Field Solution Method Elliptic Difference Equations with General Boundary Conditions," under preparation for submission to *Numerical Heat Transfer*.
22. Stone, H.L., "Iterative Solution of Implicit Approximation of Multidimensional Partial Differential Equations," *SIAM J. Num. Annual.*, vol. 5, 1968.
23. Ghia, U., Ghia, K.N., and Shin, C.T., "High-Re Solutions for Incompressible Flow Using the Navier-Stokes Equations and a Multi-Grid Method," *J. Comput. Phys.*, vol. 38, pp. 387-411, 1982.
24. Armaly, B.F., Durst, F., Pereira, J.C.F., and Schönung, B., "Experimental and Theoretical Investigation of Backward-Facing Step Flow," *J. Fluid Mech.*, vol. 127, pp. 473-496, 1983.
25. Laufer, J., "The Structure of Turbulence in Fully Developed Pipe Flow," NACA TN-2954, Washington, June 1983.
26. Samimy, M., Nejad, A.S., Langenfeld, C.A., Craig, R.R., and Vanka, S.V., "Isothermal Swirling Flow in a Dump Combustor," AIAA-87-1352, 1987.
27. de Wahl Davis, G., "Natural Convection in a Square Cavity-A Benchmark Solution," *Int. J. Numerical Methods in Fluids*, vol. 3, pp. 249-264, 1983.
28. Schefer, R.W. and Dibble, R.W., "Rayleigh Scattering

Measurements of Mixture Fraction in a Turbulent Non-Reacting Propane Jet," AIAA-86-0278, 1986.

NRC FORM 335 (2 84) NRCM 1102, 3201, 3202

U.S. NUCLEAR REGULATORY COMMISSION

BIBLIOGRAPHIC DATA SHEET

SEE INSTRUCTIONS ON THE REVERSE

1 REPORT NUMBER (Assigned by TIDC, add Vol. No., if any)

NUREG/CR-5233

2 TITLE AND SUBTITLE

A Computer Code for Fire Protection and Risk Analysis of Nuclear Plants

3 LEAVE BLANK

4 DATE REPORT COMPLETED

MONTH	YEAR
June	1988

5 AUTHOR(S)

Ashok K. Singhal, Sami D. Habchi, and Andrzej J. Przekwas

6 DATE REPORT ISSUED

MONTH	YEAR
September	1988

7 PERFORMING ORGANIZATION NAME AND MAILING ADDRESS (Include Zip Code)

CFD Research Corporation
3313 Bob Wallace Avenue, Suite 205
Huntsville, Alabama 35805

8 PROJECT/TASK/WORK UNIT NUMBER

9 FIN OR GRANT NUMBER

D2041

10 SPONSORING ORGANIZATION NAME AND MAILING ADDRESS (Include Zip Code)

Division of Engineering
Office of Nuclear Regulatory Research
U.S. Nuclear Regulatory Commission
Washington, DC 20555

11a TYPE OF REPORT

Final Report for SBIR Phase I Study

b PERIOD COVERED (Inclusive dates)

Oct. '87 - June '88

12 SUPPLEMENTARY NOTES

13 ABSTRACT (200 words or less)

A fire modeling computer code has been developed with sufficient flexibility for accurate representations of geometry, ventilation and other conditions as may be present in cable rooms, control rooms, and other enclosures in nuclear power plants. The computer code is capable of three-dimensional, transient, turbulent flow and heat transfer calculations with chemical reaction and radiation. The code has a modular structure, specifically designed for fire problems.

The code employs the latest relevant finite-volume solution techniques. The code has been applied to a series of benchmark problems and a recent fire test problem. This has confirmed the feasibility of the fire code. Considerable further work is needed to enhance the physical models (to improve the realism of predicted solutions) and to validate and document the final code. Specific recommendations are made for Phases II and III of the Project.

14 DOCUMENT ANALYSIS - a KEYWORDS/DESCRIPTORS

Fire Safety
Field Model
Fire Modeling
Computer Simulation
Fire Protection

b IDENTIFIERS/OPEN-ENDED TERMS

15 AVAILABILITY STATEMENT

Unlimited

16 SECURITY CLASSIFICATION

(This page) Unclassified

(This report) Unclassified

17 NUMBER OF PAGES

18 PRICE

NUREG/CR-5233 A COMPUTER CODE FOR FIRE PROTECTION AND RISK ANALYSIS OF NUCLEAR PLANTS SEPTEMBER 1988